F49620-95-1-0028

SYNTHETIC SEISMOGRAMS IN HETEROGENEOUS ELASTIC WAVEGUIDES AND APPLICATIONS IN INVESTIGATING LG-WAVE PROPAGATION

R.S. Wu
S. Jin
X.B. Xie
T. Lay

University of California/Santa Cruz
Institute of Tectonics
Santa Cruz, CA 95064

March 20, 1998

Final Technical Report

AFOSR/NM
AFOSR/PKA
110 DUNCAN AVENUE B115
BOLLING AFB DC 20332-8050

REPORT DOCUMENTATION PAGE

Form Approved
OMB No. 074-0188

1. AGENCY USE ONLY (Leave blank)	2. REPORT DATE	3. REPORT TYPE AND DATES COVERED
	March 20, 1998	Final Tech Report, Oct 10,94-Sep 30,97

4. TITLE AND SUBTITLE
Synthetic seismograms in heterogeneous elastic waveguides and applications in investigating Lg-wave propagation

5. FUNDING NUMBERS
F49620-95-1-0028

6. AUTHOR(S)
R.S. Wu
S. Jin
X.B. Xie
T. Lay

7. PERFORMING ORGANIZATION NAME(S) AND ADDRESS(ES)
Institute of Tectonics
University of California
1156 High Street
Santa Cruz, CA 95064

8. PERFORMING ORGANIZATION REPORT NUMBER

9. SPONSORING / MONITORING AGENCY NAME(S) AND ADDRESS(ES)
AFOSR/NM
110 Duncan Avenue Room B115
Bolling AFB DC 20332-8080

10. SPONSORING / MONITORING AGENCY REPORT NUMBER

11. SUPPLEMENTARY NOTES

12a. DISTRIBUTION / AVAILABILITY STATEMENT
Approved for public release; distribution unlimited

12b. DISTRIBUTION CODE

13. ABSTRACT ***(Maximum 200 Words)***

This study is aimed at development and application of a new wave propagation and modeling method for regional waves in heterogeneous crustal waveguides using one-way wave approximation. As the first step, we solve the 2D SH-wave problem. A half-space GSP (Generalized Screen Propagator) is formulated for the SH half space problem. We apply our method to simulating regional wave propagation in different types of complex crustal waveguides including those with small-scale random heterogeneities and random rough interfaces of sedimentary layers. Synthetic seismograms and snapshots are shown to facilitate the study of path effects of Lg waves. Slowness domain analysis is especially useful in investigating energy transfer in crustal waveguides and for determining which part of the energy can be trapped in the waveguide. The influence of crustal heterogeneities and rough interfaces on Lg amplitude attenuation and Lg coda formation are studied.

14. SUBJECT TERMS		15. NUMBER OF PAGES
Seismic wave propagation	Lg wave	45
CTBT	Generalized screen method	16. PRICE CODE

17. SECURITY CLASSIFICATION OF REPORT	18. SECURITY CLASSIFICATION OF THIS PAGE	19. SECURITY CLASSIFICATION OF ABSTRACT	20. LIMITATION OF ABSTRACT
Unclassified	Unclassified	Unclassified	SAR

Contents

Abstract

This study is aimed at development and application of a new 3D wave propagation and modeling method for regional waves in heterogeneous crustal waveguides using one-way wave approximation. The great advantages of one-way propagation methods are the fast speed of computation, often by several orders of magnitude faster than the full-wave finite-difference and finite-element methods, and the huge savings in internal memory. As the first step, we solve the 2D SH-wave problem. A half-space GSP (Generalized Screen Propagator) is formulated for the SH half space problem. Two versions of the half-space GSP are derived: the wide-angle pseudo-screen and the phase-screen. The treatment of the Moho discontinuity is also discussed. Comparisons with a wavenumber integration method for flat crustal models and a finite-difference algorithm for heterogeneous models show excellent agreement. For a model with propagation distance of 250 km, dominant frequency at 0.5 Hz, the GSP method is about 300 times faster than the finite-difference method with a similar accuracy. These comparisons demonstrate the accuracy and efficiency of the method. We apply our method to simulating regional wave propagation in different types of complex crustal waveguides including those with small-scale random heterogeneities and random rough interfaces of sedimentary layers. Synthetic seismograms and snapshots are shown to facilitate the study of path effects of Lg waves. Slowness domain analysis is especially useful in investigating energy transfer in crustal waveguides and for determining which part of the energy can be trapped in the waveguide. The influence of crustal heterogeneities and rough interfaces on Lg amplitude attenuation and Lg coda formation are studied. It is found that small scale heterogeneities and rough interfaces can scatter the Lg waves out of the guided modes causing leakage into the mantle. The leakage loss due to scattering can be an important factor for Lg attenuation and blockage.

1 Introduction

The study of path effects of complex structures and heterogeneities on the excitation and propagation of regional phases in different areas remains critical for many seismological problems, such as the study of crustal structures and the discrimination and yield estimation for low-yield nuclear test monitoring. An ideal numerical method for investigating regional wave propagation should have the capabilities to deal with crustal models that include horizontal and vertical variations with scales from geological boundaries to small scatterers, including random heterogeneities, as well as handling 3D Q structures. For the purpose of monitoring the CTBT (Comprehensive Test Ban Treaty) at regional distances, simulation algorithms are desirable for generating synthetic waveforms for high frequencies up to 25 Hz at distance greater than 1000 km.

Substantial efforts have been made in modeling regional wave propagation. Methods based on layered earth models, such as the reflectivity and mode summation methods (e.g. Bouchon et al., 1985, Kennett, 1989, 1990; Maupin, 1989; Baumgardt, 1990; Campillo, 1990; Campillo and Paul, 1992; Campillo et al., 1993; Gibson et al., 1994) have very high efficiency and can be applied to relatively high frequencies, but they can be used only for very simplified cases with layered or smoothly varying layered models, and lack the capability to simulate more realistic crustal waveguides. Modeling techniques that can treat realistic 3D heterogeneous media rather than smoothly varying layered media are needed to test and study many observations and hypotheses. Sudden changes of crustal thickness, strong lateral variations and irregular 3D heterogeneities are among the problems requiring new modeling methods. As pointed out by Campillo et al. (1993), actual Lg amplitudes were reduced more than 10 times for paths passing through an anomalous zone on the east side of the Alpine range, while the modeling results using existing methods (including the effect of known large-scale lateral structural variation) only account for 20 - 30 % of the amplitude reduction. Other mechanisms such as the scattering and attenuation by small-scale heterogeneities must be taken into account.

Finite-difference methods (e.g., Xie and Lay, 1994; Goldstein et al., 1996; Jih 1996) and

pseudo-spectral methods (e.g., Kosloff et al., 1990; Orrey et al, 1996; Schatzman, 1996) are very flexible. Theoretically they can deal with arbitrarily heterogeneous media. However, the capability of the present day computers usually restricts them to short propagation ranges and relatively low frequencies, which prevents them from being applied to more realistic models.

Recently, the generalized screen method has been introduced into seismic wave simulations. The generalized screen method is based on the one-way wave equation and the one-return approximation. The one-way wave propagator GSP (Generalized Screen Propagator) neglects backscattered waves, but correctly handles all the forward multiple-scattering effects, e.g., focusing/defocusing, diffraction, interference, and conversion between different wave types. The one-return approximation is also called the de Wolf approximation (De Wolf, 1971, 1985), which neglects the reverberation between screens and can simulate multiple-forescattering-single-backscattering (MFSB). Significant progress has been made on the development of an Elastic Complex Screen (ECS) method for modeling elastic wave propagation and scattering in arbitrarily complicated structures (Wu, 1994, 1996; Xie and Wu, 1995, 1996). The method is two to three orders of magnitude faster than the elastic finite-difference method for medium size 3D problem. The screen method has been successfully used in forward modeling (Wu, 1994; Xie and Wu 1995, 1996; Wu and Huang, 1995) and as backpropagators for seismic wave imaging/migration in both acoustic and elastic media (e.g. Wu and Xie 1994; Huang and Wu 1996). In the crustal waveguide environment, major wave energy is carried by forward propagating waves, including forward scattered waves, and therefore the neglect of backscattered waves in the propagation will not change the main features of regional waves in most cases. By neglecting backscattering in the theory, the method becomes a forward marching algorithm in which the next step of propagation depends only on the present values of the wavefield in a transverse cross-section and the heterogeneities between the two cross-sections. The saving of computing time and storage is enormous and makes it a viable method for large 3D elastic wave propagation problems.

As the first step, Wu, Jin and Xie (1997) introduced the GSP method to simulate and investigate SH Lg-wave propagation. In this report, we will discuss many applications of this

method to complicated crustal waveguide structures. In section 2 we first give the wide-angle pseudo-screen formulas for one-way SH-waves in a half space. Then a phase-screen algorithm is obtained under the small-angle forward scattering approximation. The treatment of the Moho discontinuity is also discussed. In section 3, we compare the simulation results of the method with those from wavenumber integration and finite-difference methods. For a flat crustal model, for which the wavenumber integration (WI) method (reflectivity method) is considered as accurate, our result shows excellent agreement with the WI method. For a heterogeneous crustal model with propagation distance of 250 km and dominant frequency of 0.5 Hz, the GSP method is about 300 times faster than the finite-difference method with a similar accuracy. These comparisons demonstrate the accuracy and efficiency of the half-space GSP method. In section 4 we apply our method to regional wave propagation in different types of complex crustal waveguides including those with small-scale random heterogeneities and random rough interfaces of sedimentary layers. The influence of these heterogeneities and rough interfaces on Lg amplitude attenuation and Lg coda formation are shown to be significant. Section 5 focuses on the slowness domain analysis. Although investigating wave propagation in space-time domain is more straightforward, slowness domain analysis provides a clearer picture of energy propagating directions as well as better criteria for energy partitioning. Conclusion and discussions are given in the final section.

2 Theory

First we derive the wide-angle screen formula for the 2D SH-wave one-way propagation in an elastic half space. The equation of motion in a linear, heterogeneous elastic medium can be written as (Aki and Richards, 1980)

$$-\omega^2 \rho(\mathbf{r})\mathbf{u}(\mathbf{r}) = \nabla \cdot \sigma(\mathbf{r}) \tag{1}$$

where ω is the frequency, $\mathbf{r} = (x, z)$ is a 2D position vector, $\mathbf{u}$ is the displacement vector, σ is the stress tensor (dyadic) and ρ is the density of the medium. Here we assume no body force exists in the medium. For an isotropic 2D elastic medium, the SH and the P-SV waves are

decoupled. In this article we will treat only the SH problem to demonstrate the applicability of screen propagators to crustal waveguide problems.

2.1 General wide-angle formulation

For a 2D SH problem, only the y-component of the displacement field exists and the divergence of the stress tensor can be simplified into

$$\begin{aligned} \nabla \cdot \sigma(\mathbf{r}) &= \nabla \cdot (\mu \nabla u) \\ &= \frac{\partial}{\partial x}[\mu(\mathbf{r})\frac{\partial}{\partial x}u] + \frac{\partial}{\partial z}[\mu(\mathbf{r})\frac{\partial}{\partial z}u] \end{aligned} \tag{2}$$

where $u = u_y$, ∇ is the 2D gradient operator, and μ is the shear rigidity. We decompose the parameters of the elastic medium and the total wave field into

$$\begin{aligned} \rho &= \rho_0 + \delta\rho \\ \mu &= \mu_0 + \delta\mu \\ u &= u^0 + U \end{aligned} \tag{3}$$

where ρ_0 and μ_0 are the parameters of the background medium, $\delta\rho$ and $\delta\mu$ are the corresponding perturbations, u^0 is the primary field and U is the scattered field. Then the SH wave equation can be rewritten as

$$\mu_0 \nabla^2 u + \omega^2 \rho_0 u = -[\omega^2 \delta\rho u + \nabla \cdot \delta\mu \nabla u] \,, \tag{4}$$

or

$$(\nabla^2 + k^2)u(\mathbf{r}) = -k^2 F(\mathbf{r})u(\mathbf{r}) \,, \tag{5}$$

where $k = \omega/v$ is the wavenumber in the background medium and v is the background S wave velocity defined by

$$v = \sqrt{\mu_0/\rho_0} \tag{6}$$

In the right hand side of (5), $F(\mathbf{r})$ is a perturbation operator

$$F(\mathbf{r}) = \varepsilon_\rho(\mathbf{r}) + \frac{1}{k^2}\nabla \cdot \varepsilon_\mu \nabla \,, \tag{7}$$

with

$$\varepsilon_\rho(\mathbf{r}) = \frac{\delta\rho(\mathbf{r})}{\rho_0}\,, \tag{8}$$

$$\varepsilon_\mu(\mathbf{r}) = \frac{\delta\mu(\mathbf{r})}{\mu_0}\,. \tag{9}$$

Equation (5) is a scalar Helmholtz equation. With a half-space scalar Green's function g^h, the scattered field U can be written as

$$U(\mathbf{r}_1) = k^2 \int_V d^2\mathbf{r} g^h(\mathbf{r}_1;\mathbf{r}) F(\mathbf{r}) u(\mathbf{r})\,, \tag{10}$$

where the 2D volume integration is over the volume V including all the heterogeneities in the modeling space. Using the Gauss divergence theorem the above equation reduces to (cf. Wu, 1994)

$$\begin{aligned} U(\mathbf{r}_1) &= k^2 \int_v d^2\mathbf{r} \Big\{ g^h(\mathbf{r}_1;\mathbf{r})\varepsilon_\rho(\mathbf{r})u(\mathbf{r}) \\ &- \frac{1}{k^2}\nabla g^h(\mathbf{r}_1;\mathbf{r})\cdot\varepsilon_\mu(\mathbf{r})\nabla u(\mathbf{r})\Big\} \end{aligned} \tag{11}$$

Under the forward-scattering approximation, or more generally the multiple-forescattering-single-backscattering (MFSB) approximation (De Wolf, 1971, 1985; Wu and Huang, 1995; Wu, 1996), the total field and Green's function under the integration in the above equation can be replaced by their forward-scattering approximated counterparts, and the field can be calculated by a one-way marching algorithm along the x-direction using a dual domain technique. We will derive in the following the dual domain expressions of the marching algorithm for the heterogeneous half-space case.

For each step of the marching algorithm under the forward-scattering approximation, the total field at x_1 is calculated as the sum of the primary field which is the field free-propagated in the half-space from x' to x_1, and the scattered field caused by the heterogeneities in the thin-slab between x' and x_1. The thickness of the slab should be made thin enough to ensure the validity of the local Born approximation. Under this condition, the Green's function can be approximated by the homogeneous half-space Green's function. The latter can be obtained by the image method (Morse and Feshbach, 1953). The stress should vanish at the

free surface $z = 0$, leading to $\mu \partial u/\partial z = 0$, a Neumann boundary condition. Therefore, we have

$$g_0^h(\mathbf{r}_1; \mathbf{r}) = g_0(\mathbf{r}_1; \mathbf{r}) + g_0(\mathbf{r}_1; \mathbf{r}*) \tag{12}$$

where g_0 is the infinite homogeneous Green's function and $\mathbf{r}*$ is the mirror point of $\mathbf{r}$ with respect to the free surface.

Taking the Fourier transform of Eq. (11) along z_1, for the case of a thin-slab we have

$$\begin{aligned} U(x_1, K_z) &= k^2 \int_{x'}^{x_1} dx \int_0^\infty dz \{ g_0^h(x_1, K_z; x, z) \varepsilon_\rho(x, z) u_0(x, z) \\ &- \frac{1}{k^2} \nabla g_0^h(x_1, K_z; x, z) \cdot \varepsilon_\mu(x, z) \nabla u(x, z) \} \end{aligned} \tag{13}$$

We know the free space Green's function in wavenumber domain (Wu and Huang, 1995; Wu, 1996)

$$g_0(x_1, K_z; x, z) = \frac{i}{2\gamma} e^{i\gamma(x_1 - x)} e^{-iK_z z} \tag{14}$$

with

$$\gamma = \sqrt{k^2 - K_z^2}\,, \tag{15}$$

Therefore,

$$\begin{aligned} g_0^h(x_1, K_z; x, z) &= g_0(x_1, K_z; x, z) + g_0(x_1, K_z; x, -z) \\ &= \frac{i}{2\gamma} e^{i\gamma(x_1 - x)} [e^{-iK_z z} + e^{+iK_z z}] \\ &= \frac{i}{2\gamma} e^{i\gamma(x_1 - x)} 2\cos(K_z z) \end{aligned} \tag{16}$$

In a similar way we can obtain

$$\nabla g_0(x_1, K_z; x, z) = \frac{1}{2\gamma} (\gamma \hat{e}_x + K_z \hat{e}_z) e^{i\gamma(x_1 - x)} e^{-iK_z z} \tag{17}$$

and

$$\begin{aligned} \nabla g_0^h &= \frac{\partial}{\partial x} g_0^h \hat{e}_x + \frac{\partial}{\partial z} g_0^h \hat{e}_z \\ &= \frac{1}{2} e^{i\gamma(x_1 - x)} \{ \hat{e}_x 2\cos(K_z z) - \hat{e}_z (K_z/\gamma) 2i \sin(K_z z) \} \end{aligned} \tag{18}$$

where $\hat{e}_x$ and $\hat{e}_z$ are unit vectors in the x and z directions, respectively.

Substitute g_0^h and ∇g_0^h into (13), leading to

$$\begin{aligned} U(x_1, K_z) &= U_\rho(x_1, K_z) + U_\mu(x_1, K_z) \\ U_\rho(x_1, K_z) &= \frac{ik}{2}\int_{x'}^{x_1} dx e^{i\gamma(x_1-x)} \int_0^\infty dz 2\cos(K_z z)\frac{k}{\gamma}\varepsilon_\rho(x,z)u_0(x,z) \\ U_\mu(x_1, K_z) &= -\frac{ik}{2}\int_{x'}^{x_1} dx e^{i\gamma(x_1-x)} \\ &\quad \int_0^\infty dz[2\cos(K_z z)\bar{\partial}_x u_0 - 2i\sin(K_z z)\frac{K_z}{\gamma}\bar{\partial}_z u_0]\varepsilon_\mu(x,z) \end{aligned} \tag{19}$$

where

$$\begin{aligned} \bar{\partial}_x &= \frac{1}{ik}\frac{\partial}{\partial x} \\ \bar{\partial}_z &= \frac{1}{ik}\frac{\partial}{\partial z} \end{aligned} \tag{20}$$

are dimensionless partial derivatives. Or we can write these equations as

$$U_\rho(x_1, K_z) = \frac{ik}{2}\int_{x'}^{x_1} dx e^{i\gamma(x_1-x)}\mathcal{C}[\frac{k}{\gamma}\varepsilon_\rho(z)u_0(z)] \tag{21}$$

$$U_\mu(x_1, K_z) = -\frac{ik}{2}\int_{x'}^{x_1} dx e^{i\gamma(x_1-x)}\left\{\mathcal{C}[\varepsilon_\mu(z)\bar{\partial}_x u_0(z)] - i\mathcal{S}[\frac{K_z}{\gamma}\varepsilon_\mu(z)\bar{\partial}_z u_0(z)]\right\} \tag{22}$$

where $\mathcal{C}[f(z)]$ and $\mathcal{S}[f(z)]$ are cosine and sine transforms, defined by

$$\begin{aligned} \mathcal{C}[f(z)] &= \int_0^\infty dz 2\cos(K_z z)f(z) \\ \mathcal{S}[f(z)] &= \int_0^\infty dz 2\sin(K_z z)f(z) \end{aligned} \tag{23}$$

for forward transforms, and

$$\begin{aligned} \mathcal{C}^{-1}[f(K_z)] &= \frac{1}{2\pi}\int_0^\infty dK_z 2\cos(K_z z)f(K_z) \\ \mathcal{S}^{-1}[f(K_z)] &= \frac{1}{2\pi}\int_0^\infty dK_z 2\sin(K_z z)f(K_z) \end{aligned} \tag{24}$$

for inverse transforms.

In Eqs. (21) and (22), u_0, $\bar{\partial}_x u_0$ and $\bar{\partial}_z u_0$ can be calculated by

$$\begin{aligned} u_0(x,z) &= \frac{1}{2\pi}\int_{-\infty}^\infty dK_z' e^{iK_z' z} e^{i\gamma'(x-x')}u_0(x', K_z') \\ &= \mathcal{C}^{-1}[e^{i\gamma'(x-x')}u_0(x', K_z')] \end{aligned} \tag{25}$$

and

$$\begin{aligned} \bar{\partial}_x u_0(x,z) &= \mathcal{C}^{-1}[e^{i\gamma'(x-x')}\frac{\gamma'}{k}u_0(x',K_z')] \\ \bar{\partial}_z u_0(x,z) &= i\mathcal{S}^{-1}[e^{i\gamma'(x-x')}\frac{K_z'}{k}u_0(x',K_z')] \end{aligned} \tag{26}$$

Eqs. (21), (22), (25) and (26) are the dual-domain expressions of the wide-angle screen propagator for half-space SH problems.

2.2 Implementation procedure for the half-space wide-angle screen propagator

Under the forward-scattering approximation we can update the total field with a marching algorithm in the forward direction. The half-space model can be sliced into thin-slabs perpendicular to the propagation direction. Weak scattering condition holds for each thin-slab. For each slab-step forward, the forward-scattered field by the thin-slab is calculated and added to the primary field so that the updated field becomes the incident field for the next thin-slab. The procedure can be summarized as follows.

1. Cosine transform the incident fields at the entrance of each thin-slab into wavenumber domain.

2. Free propagate in wavenumber domain and calculate the primary field and its gradient within the slab.

3. At each horizontal position within the slab, inverse cosine/sine transform the primary field and its gradients into space domain (25 and 26), and then interact with the medium perturbations ε_ρ and ε_μ.

4. Cosine/sine transform the distorted fields into wavenumber domain and perform the divergence operations to get the scattered fields (21 and 22).

5. Calculate the primary field at the slab exit and add to the scattered field to form the total field as the incident field at the entrance of the next thin-slab.

6. Continue the procedure iteratively.

2.3 Small angle approximation and the phase-screen propagator

When the energy of crustal guided waves is carried mainly by small-angle waves (with respect to the horizontal direction), the small angle approximations can be invoked to simplify the theory and calculations. Let us first consider the calculations for U_μ. Substitute (26) into (22), resulting in

$$\begin{aligned} U_\mu(x_1, K_z) &= -\frac{ik}{2}\int_{x'}^{x_1} dx e^{i\gamma(x_1-x)}\frac{1}{2\pi}\int_0^\infty dK_z' e^{i\gamma'(x-x')}\int_0^\infty dz \\ &\quad \left\{2\cos(K_z z)\varepsilon_\mu(z) 2\cos(K_z' z)(\frac{\gamma'}{k})\right. \\ &+ \left. 2\sin(K_z z)\varepsilon_\mu(z) 2\sin(K_z' z)(\frac{K_z}{\gamma})(\frac{K_z'}{k})\right\} u_0(x', K_z') \end{aligned} \tag{27}$$

This is the local Born scattering in wavenumber domain. The above equation can be written as

$$U_\mu(x_1, K_z) = \mathbf{A}_\mu u_0(x', K_z') \tag{28}$$

where $\mathbf{A}_\mu$ is an operator. In the discrete form, it is a matrix, whose elements are incident and outgoing (scattered) wavenumbers dependent. For small-angle waves, $K_z \ll \gamma \approx \gamma' \approx k$. The second term of Eq. (27) is a second order small quantity compared with the first term, and therefore can be neglected in this case. Then we have

$$\begin{aligned} U(x_1, K_z) &= U_\rho(x_1, K_z) + U_\mu(x_1, K_z) \\ &= \frac{ik}{2} e^{i\gamma(x_1-x')}\frac{1}{2\pi}\int_0^\infty dK_z' 2\cos(K_z' z)\int_0^\infty dz 2\cos(K_z z) \\ &\quad \int_{x'}^{x_1} dx e^{i(\gamma-\gamma')(x-x')}\left[(\frac{k}{\gamma})\varepsilon_\rho(z) - (\frac{\gamma'}{k})\varepsilon_\mu(z)\right] u_0(x', K_z') \\ &\approx ike^{i\gamma(x_1-x')}\mathcal{C}\left[S_s(z)u_0(x', z)\right] \end{aligned} \tag{29}$$

where

$$\begin{aligned} S_s(z) &= \frac{1}{2}\int_{x'}^{x_1} dx[\varepsilon_\rho(x, z) - \varepsilon_\mu(x, z)] \\ &\approx \Delta x \bar{\varepsilon}_s(z) \end{aligned} \tag{30}$$

where $\bar{\varepsilon}_s(z)$ is the average S-wave slowness perturbation over the thin-slab at depth z, $\bar{\varepsilon}_s(z) = \frac{1}{x_1-x'}\int_{x'}^{x_1} dx\frac{s(x,z)-s_0}{s_0}$ with $s(x,z) = \frac{1}{v(x,z)}$, $\Delta x = (x_1 - x')$ is the thin-slab thickness. Here S_s is the corresponding slowness screen for the half-space thin-slab. Eq. (29)

is the screen approximation of the half-space SH problem. Summing up the primary and scattered fields and invoking the Rytov transform result in the dual-domain expression of phase-screen propagator for this case

$$\begin{aligned} u(x_1, K_z) &= u_0(x_1, K_z) + U(x_1, K_z) \\ &= e^{i\gamma(x_1 - x')} \int_0^\infty dz 2\cos(K_z z)[1 + ikS_s(z)]u_0(x', z) \\ &\approx e^{i\gamma(x_1 - x')} \mathcal{C}\left[e^{ikS_s(z)} u_0(x', z)\right] \end{aligned} \tag{31}$$

where $e^{ikS_s(z)}$ is the phase delay operator.

2.4 Implementation procedure for the half space phase-screen propagator

Under the phase-screen approximation, the heterogeneous half-space is represented by a series of half-screens embedded in the homogeneous background half-space. The wave propagates between screens in the wavenumber domain and interacts with the phase-screens in the space domain. The interaction is only a phase-delay operator (multiplication in space domain). The procedure can be summarized as follows.

1. Cosine transform the incident field at the starting plane into wavenumber domain and free propagate to the screen.

2. Inverse cosine transform the incident field into space domain and interact with the shear slowness screen (phase-screen) to get the transmitted field.

3. Cosine transform the transmitted field into wavenumber domain and free-propagate to the next screen.

4. Repeat the propagation and interaction screen-by-screen to the boundary of the model space.

2.5 Treatment of the Moho discontinuity

The Moho discontinuity can be treated in two ways. One is to put the impedance boundary conditions in the formulation, the other is to treat the parameter changes as perturbations

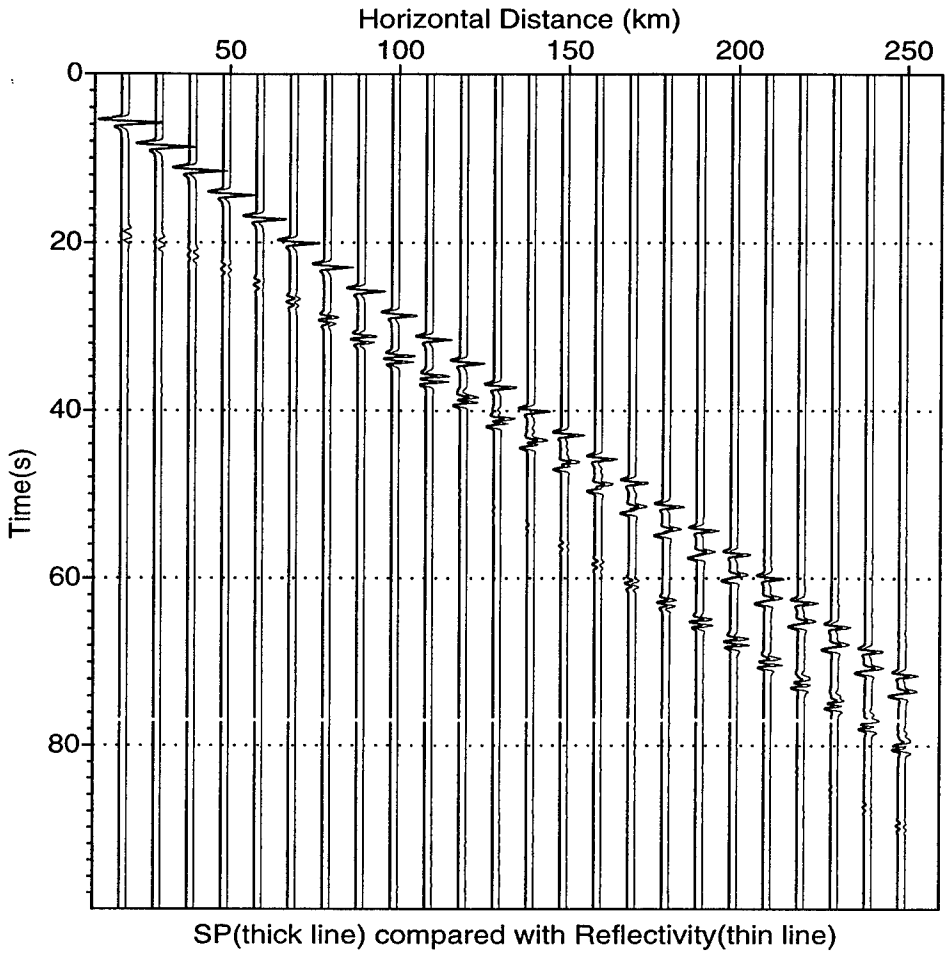

Figure 1: Comparison of synthetic seismograms along the surface calculated by the screen method (thick lines) and reflectivity method (thin lines) for a flat crustal model (32 km thick). The source function is a Ricker wavelet with dominant frequency of 1.0 Hz.

and therefore be incorporated into the screen interaction. The former has the advantage of computational efficiency. The latter has the flexibility of handling irregular interfaces. In this paper, we adopt the latter approach and check the validity of perturbation approach for the Moho discontinuity by a finite-difference algorithm.

3 Numerical verification and tests

To test the validity of the half-space GSP method (or simply call it the screen method), we have conducted extensive numerical tests and checked the results with various well known numerical methods, such as the wavenumber integration and finite-difference methods.

First, in Figure 1 we show the accuracy of the method by comparing the synthetic seismograms generated by the screen method (thick lines) with those calculated by a reflectivity method (thin lines) for a flat crustal model. The crust has a thickness of 32 km and a shear wave velocity of 3.5 km/s. The mantle beneath the crust has a shear velocity of 4.5 km/s. The source function is a Ricker wavelet with a dominant frequency of 1.0 Hz. Our results agree very well with the reflectivity method which is considered very accurate for flat layered media. The only exceptions are for near vertical reflections at very small epicentral distances where the screen method has low accuracy for extremely large scattering angles with respect to the propagation direction. However, since regional seismograms are usually recorded at large distances, this limitation does not pose any real problem for its application. Next, we show the accuracy of the method by comparing synthetic seismograms generated by this method with those generated by a finite-difference algorithm (Xie and Lay, 1994). For the finite-difference method, a fourth-order elastic SH-wave code is used to calculate the synthetic seismograms. The spatial sampling interval is 0.125 km in both vertical and horizontal directions, and the time interval is 0.015 *second*. For the screen method, the spatial sampling interval is 0.25 km in the vertical direction and the screen interval is 1.0 km. A Gaussian derivative is used as the source time function for both methods. Because of the computational intensity of the finite-difference method, we did the comparison at short propagation distances (250 km) and a relatively low frequency ($f_0 \sim 0.5$ Hz). Figure 2 gives the comparison between synthetic seismograms from the screen method and from the finite-difference method for the same flat layered model. Their agreement is excellent.

Next we show the comparison for a heterogeneous crustal model. On the top of Figure 3 is the crust model with a narrow passage ('neck' type) used to calculate synthetic seismograms. On the bottom are the synthetic seismograms along a vertical profile at an epicentral distance

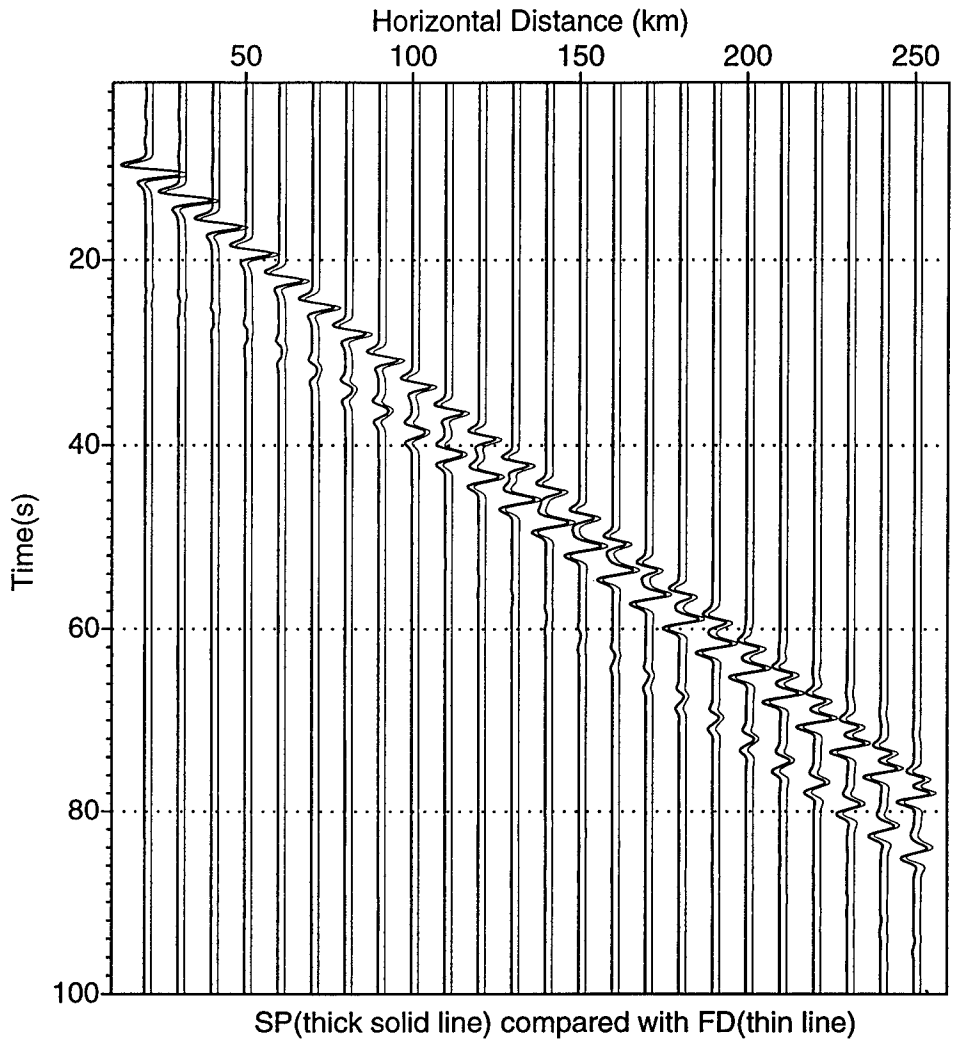

Figure 2: Comparison of synthetic seismograms along the surface calculated by the screen method (thick lines) and the fourth-order finite-difference method (thin lines) for a flat crustal model (32 km thick). The source function is a Gaussian derivative ($f_0 \sim 0.5$ Hz).

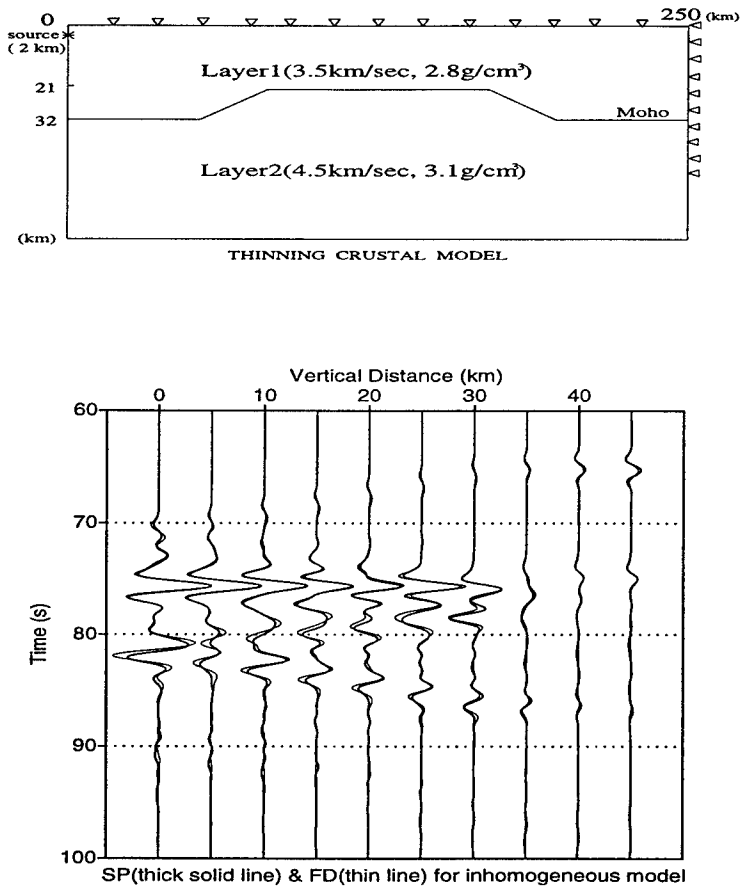

Figure 3: Comparison of synthetic seismograms along a vertical profile at the distance of 250 km calculated by the screen method (thick lines) and a finite-difference method (thin lines) for a laterally varying crustal model shown on the top panel.

of 250 km. The thin lines are from the finite-difference method and the thick lines are from the screen method. The source is located at a depth of 2 km. Excellent agreement can be seen. For this example, the GSP method took 20 CPU minutes on a SPARC-4. To obtain a similar accuracy, the finite-difference calculation took 3000 CPU minutes on a SPARC-20. The speed factor is about 300.

We have performed an accuracy comparison between the screen method and finite-difference method for different grid spacings. It was found that when the grid spacing for the finite-difference method is 0.25 km, although it still satisfies the stability criterion for the finite-difference method, there are considerable discrepancies between the results of the two methods (see the figure in Wu et al., 1997). This is due to the numerical dispersion of the finite-difference method. With a finer grid spacing of 0.125 km, the results from finite-difference converged to those of the GSP method. This shows that for wave propagation through a long crustal waveguide, the finite-difference method requires finer grid than the conventional stability criterion. The grid spacing (Δz) of the screen method for the comparison is 0.5 km, and the screen interval (Δx) is 1 km.

4 Investigating Lg-wave propagation in complex crustal structures

In this section we show some examples demonstrating the potential of the method applied to various problems of regional wave propagation.

4.1 Long range Lg propagation simulation in complex crustal waveguides

Visualize the path effects by snap shots. The high efficiency of the method permits the simulation of Lg wave propagation through long crustal wave guides. The snap-shots can be easily generated to visually analyze the path effects of Lg wave propagation. Figures 4, 5 and 6 show the snap shots calculated by the screen method for different waveguides

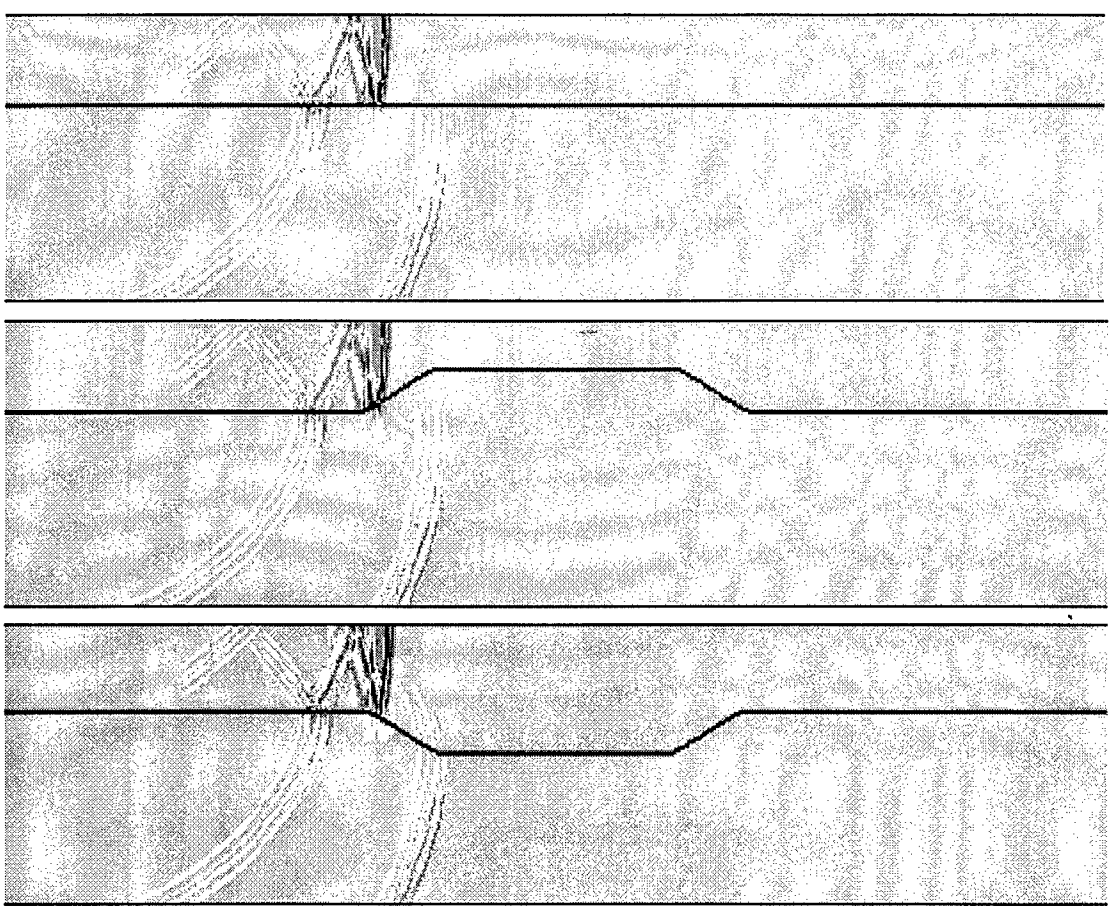

Figure 4: Snap shots at 30 *sec.* The development of mantle waves and head waves can be seen clearly.

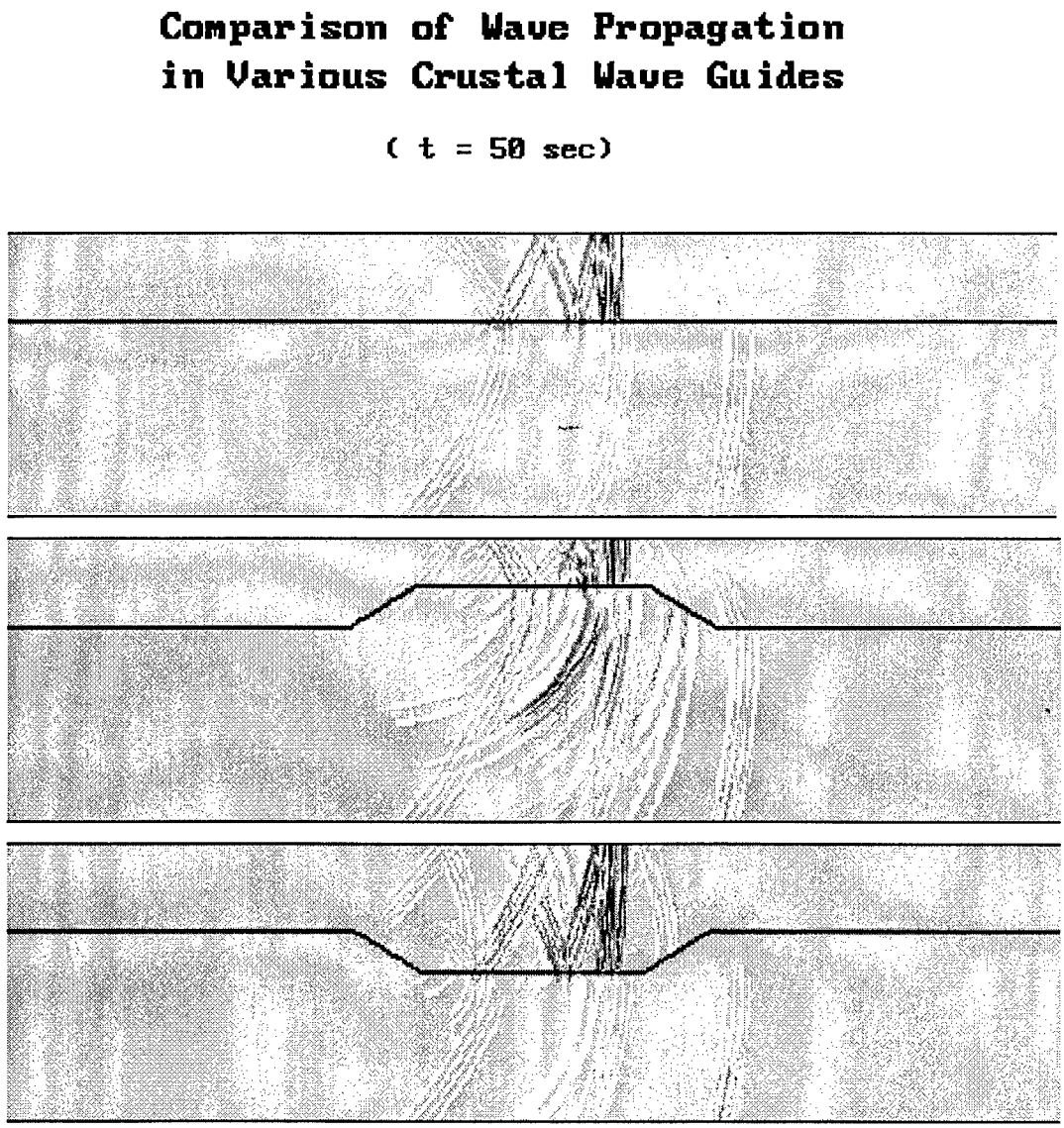

Figure 5: Snap shots at 50 *sec.* The development of mantle waves and head waves, and the influence of crust thining and thickening can be seen clearly.

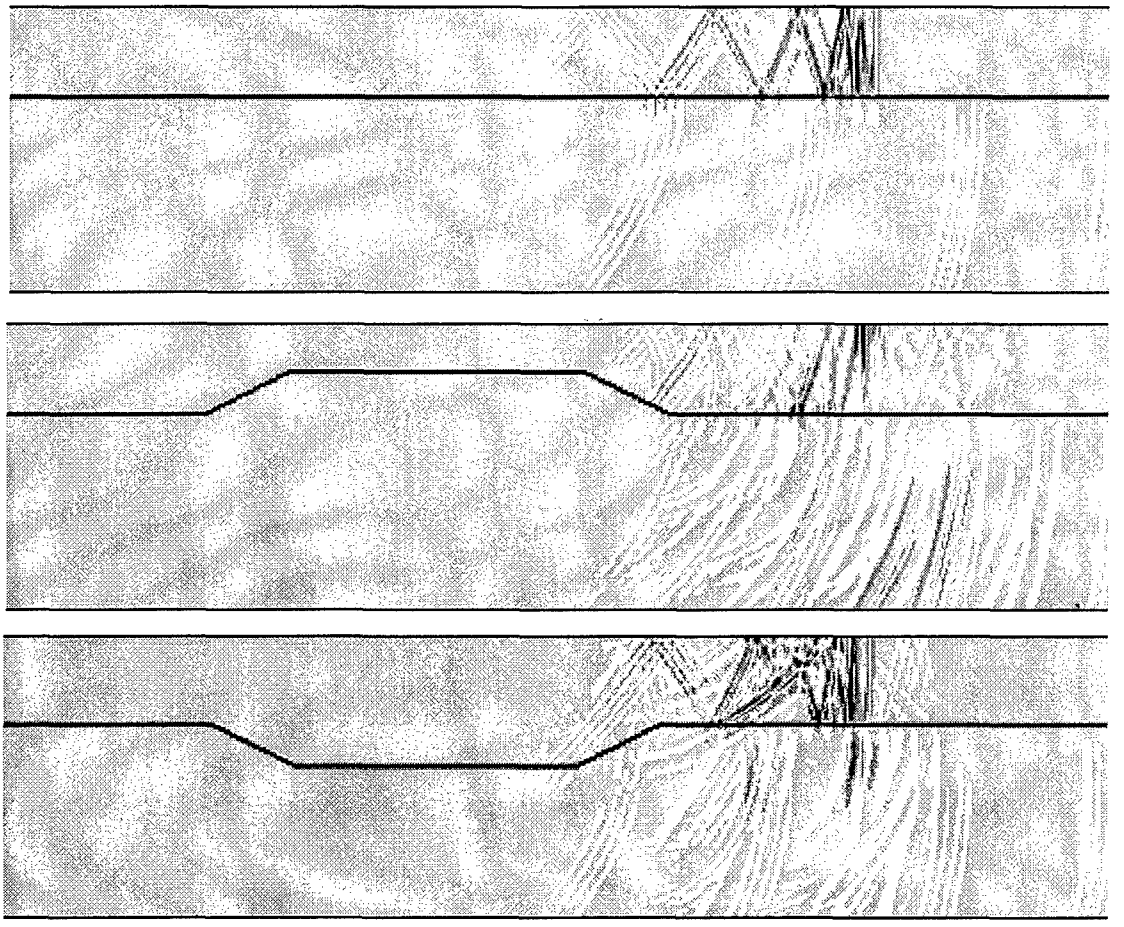

Figure 6: Snap shots at 70 *sec.* The development of mantle waves and head waves, and the influence of crust thining and thickening can be seen clearly.

at 30, 50 and 70 *sec.*, respectively. In each figure, from top to bottom are results for flat, narrowing and broadening crustal waveguides respectively. The source is located on the left boundary at a depth of 2 *km*. The development of mantle wave and head wave, as well as the formation of crustal guided waves as multiple reflections between free surface and Moho discontinuity can be clearly seen. For the inhomogeneous models, wave diffraction, leakage to the mantle, wavefront distortion and increase of wavefield complexity can also be seen clearly. From the comparison it is seen that the passage of a narrow crustal waveguide ('neck' type) has greater effect on Lg leakage than the broad passage ('belly' type). In the latter case although the wavefronts are complicated due to scattering at the edges, there is more energy trapped in the crust than the case of narrow passage in which a large percentage of energy leaks into the mantle. This example demonstrates the potential of the method as a tool for investigating the path effects of different crustal structures.

Long-range high-frequency synthetic seismograms. The following example shows the capability of this method for long range high-frequency synthetic seismograms in a laterally varying structure. Figure 7 shows the laterally varying crust model used in the calculation. Figure 8 shows the high-frequency synthetic seismograms on the surface at distances up to 1000 *km*. The center frequency $f_c = 5\ Hz$ with the maximum frequency $f_{max} = 10\ Hz$. In comparison, the low-frequency ($f_c = 1$ Hz, $f_{max} = 2$ Hz) synthetic seismograms are shown in Figure 9. It is clear that without high-frequency content, many of the distinctive features associated with Lg measurements can not be adequately modeled. In other words, a proper simulation method with the capability to generate accurate high-frequency signals is a necessity for the purpose of investigating regional phases.

4.2 The influences of random heterogeneities and rough interfaces

The importance of small-scale random heterogeneities to seismic wave propagation is well known. There are extensive publications on this subject in seismology. However, the role of random heterogeneities in Lg excitation, propagation, attenuation and blockage, is still unclear due to the complexity of the problem. The theory of wave propagation in unbounded

Parameters of Crustal Model

Layer	Vs(km/sec)	Density(g/cm)	Thickness(km)
1	3.00	2.60	1.00
2	3.46	2.80	14.00
3	3.76	3.00	22.00
4	4.65	3.30	Half-Space

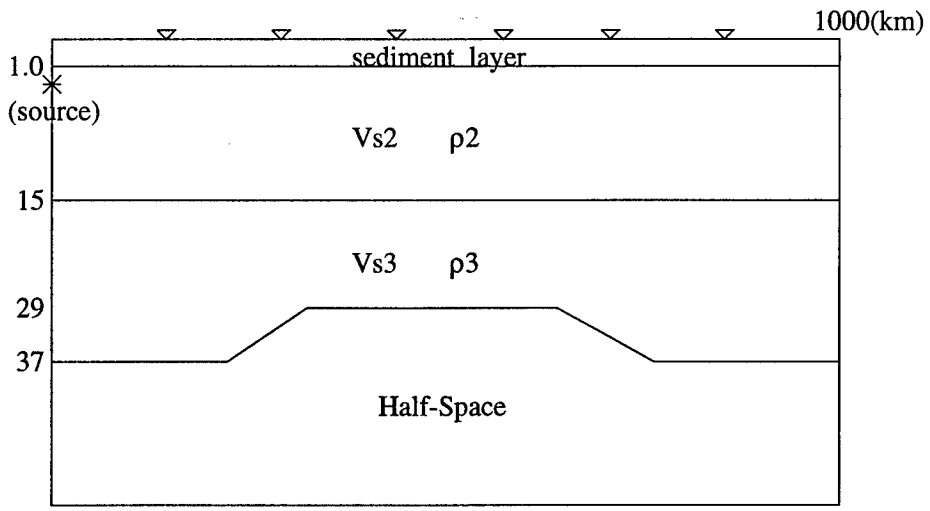

Crustal Model

Figure 7: An inhomogeneous crustal model used in the calculation of high-frequency synthetic seismograms. Shown in the upper panel are model parameters and the lower panel gives the geometry of the model. The receivers are on the surface and shown by triangles.

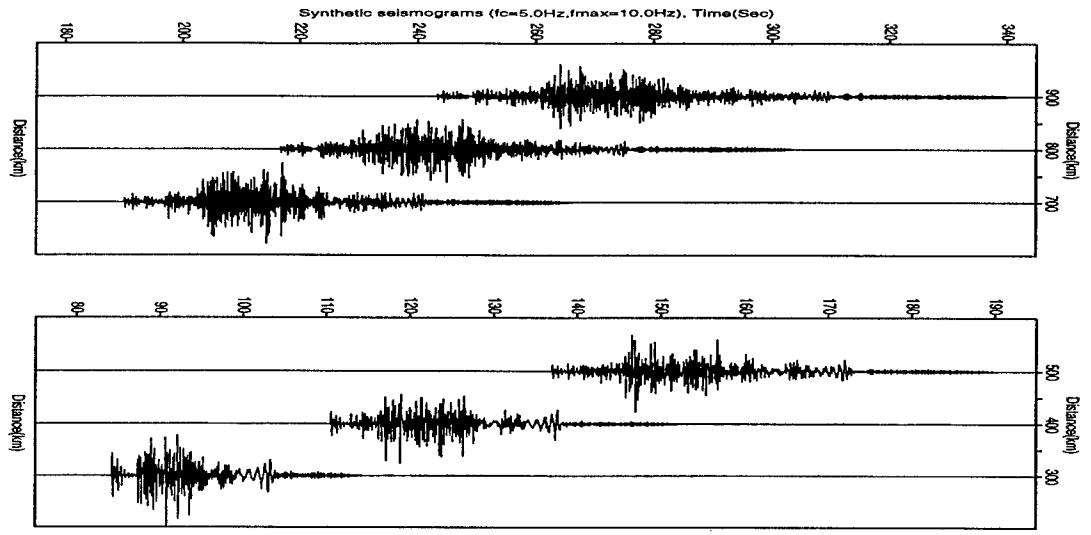

Figure 8: High-frequency ($f_c = 5$ Hz, $f_{max} = 10$ Hz) synthetic seismograms on the surface at distances up to 1000 km for an inhomogeneous crustal waveguide

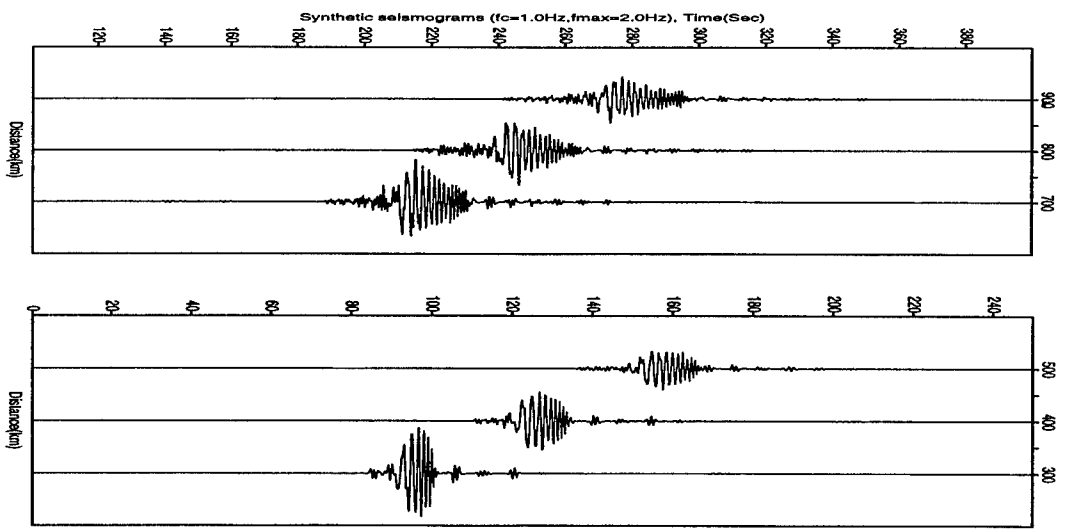

Figure 9: Low-frequency ($f_c = 1$ Hz, $f_{max} = 2$ Hz) synthetic seismograms on the surface at distances up to 1000 km for an inhomogeneous crustal waveguide

random media has been well developed. However, for waves in complex crustal waveguides with random heterogeneities, the theoretical difficulties are overwhelming, and no analytical tools are available for performing realistic calculations. Numerical simulation is an attractive alternative to the theory. Some finite-difference simulations have been conducted (e.g. Frankel and Clayton, 1986; Frankel, 1989; Xie and Lay, 1994; Jih, 1996). Limited by the computation power, however, the finite-difference results are often for short distances or low frequencies. Liu and Wu (1994) have done some numerical simulation using the phase-screen method, but the media simulated are limited to unbounded media. The development of the half-space GSP method, enables us to simulate high-frequency waves propagating in complex crustal waveguides to long distances. In the following, we will show two examples demonstrating the capability of the method.

Figure 10 shows a heterogeneous crustal model representing a 'mountain root' with small-scale random heterogeneities. On the top panel is the velocity model, and the comparisons between synthetic seismograms with and without random heterogeneities are shown on the middle and bottom panels, respectively. The heterogeneities have an exponential correlation function, with the scale length $a_x = a_z = 1.6\ km$ (in horizontal and vertical directions, respectively). The RMS velocity perturbation is 5%. The dominant frequency of the source function is 2 Hz. Figures 11 A and B show the comparison between snapshots for waves passing through the 'mountain root' with and without random heterogeneities, respectively. We see that random heterogeneities drastically increase the leakage of waves to the mantle and the complexity of the waveforms. Extensive numerical experiments will be conducted to study the different influences of various kinds of random heterogeneities. It has been shown that the crustal random heterogeneities are highly anisotropic in scale length (Levander and Holliger, 1992; Holliger and Levander, 1992; Wu et al., 1994). The influences of the random heterogeneities with different stochastic characteristics will be explored systematically.

Figure 12 shows the comparison of synthetic seismograms and snapshots for models with and without a rough interface. Shown on the first panel is a crustal model with a 1 km thick low-velocity top layer. The bottom of the low-velocity layer is a rough interface with 0.2 km RMS random depth fluctuations. The randomness has an exponential correlation function

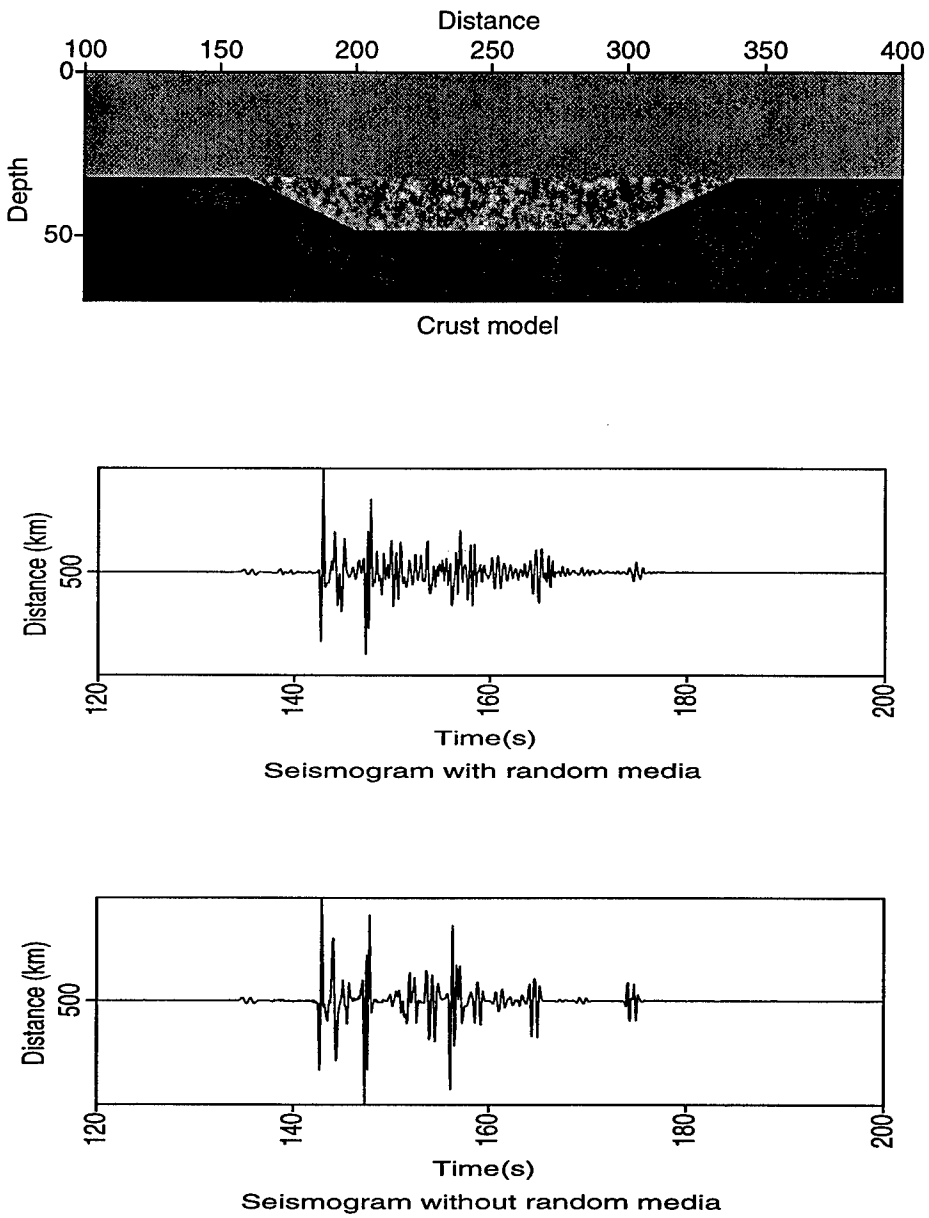

Figure 10: A heterogeneous crustal model representing a mountain root with small-scale random heterogeneities (top panel). The comparison between synthetic seismograms with and without random heterogeneities are shown on the middle and bottom panels, respectively.

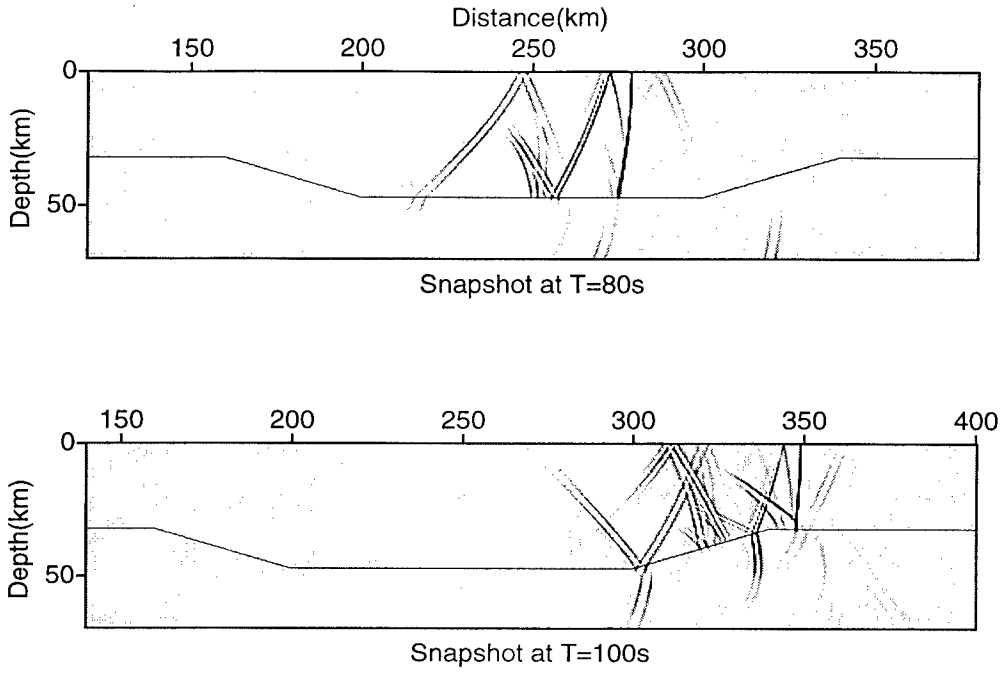

A. Snapshot for waves passing a mountain root without random heterogeneities

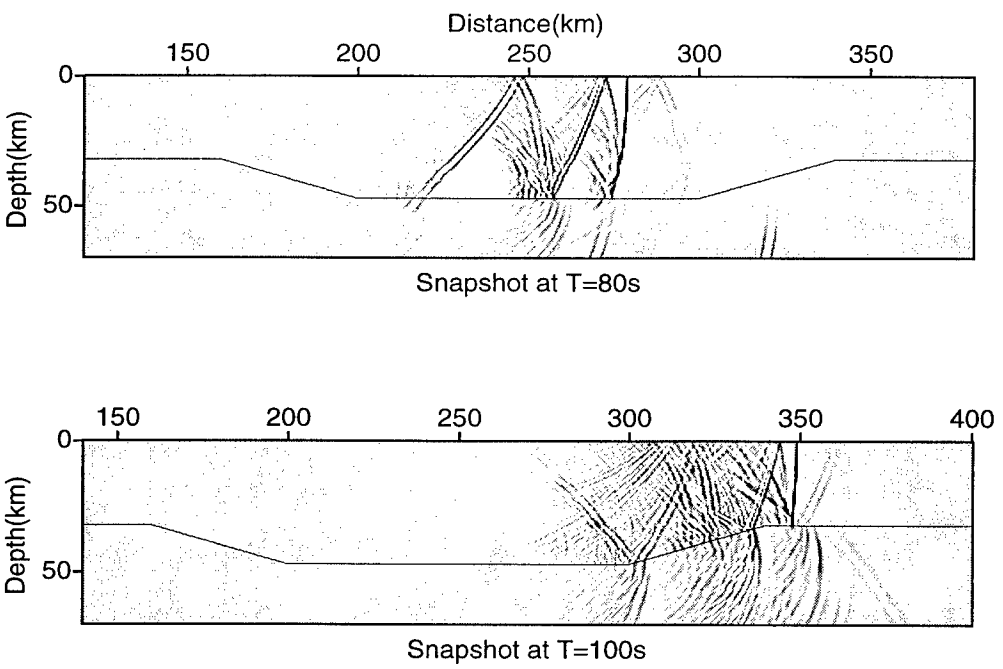

B. Snapshot for waves passing a mountain root with random heterogeneities

Figure 11: Comparison between snapshots for waves passing through a 'mountain root' with or without random heterogeneities, shown on A and B, respectively.

and a horizontal scale length of 0.5km. The second and third panels show the comparison of synthetic seismograms; the bottom two panels show the comparison of snapshots. We see that rough interfaces of sedimentary layers can also increase the mantle leakage and waveform complexity of regional waves.

5 Energy transfer and partitioning

While the wave-field snapshots discussed previously are very intuitive for assessing general feature of Lg-wave propagation, it is rather difficult, in a complex model, to investigate the energy transport by directly analyzing waveforms and snapshots. In this section, we will focus our investigation on wave energy transfer and partitioning in heterogeneous crustal waveguides.

The upper boundary of the crustal wave guide is the free surface, which is a perfect reflector. The lower boundary of the wave guide is the Moho discontinuity. For waves incident on the Moho discontinuity, part of the energy will leak into the upper mantle. However, for waves incident on the Moho with post-critical angles, total reflections occur and all the energy is reflected and trapped in the waveguide. Generally speaking, the guided energy

$$E_g = \int_{K_z<K_c} |u(K_z)|^2 dK_z \tag{32}$$

where K_c is the critical wavenumber. Scattering processes can redistribute the energy in wavenumber domain, causing the trapped energy leak to the upper mantle. Therefore investigating energy distribution versus the propagation angle, or equivalently their vertical slowness, can give a clear picture of which part of the energy can be trapped in the wave guide and which part of the energy will leak into the upper mantle. We will use a set of numerical examples and slowness analysis to investigate the interactions between Lg-waves and different types of wave guides.

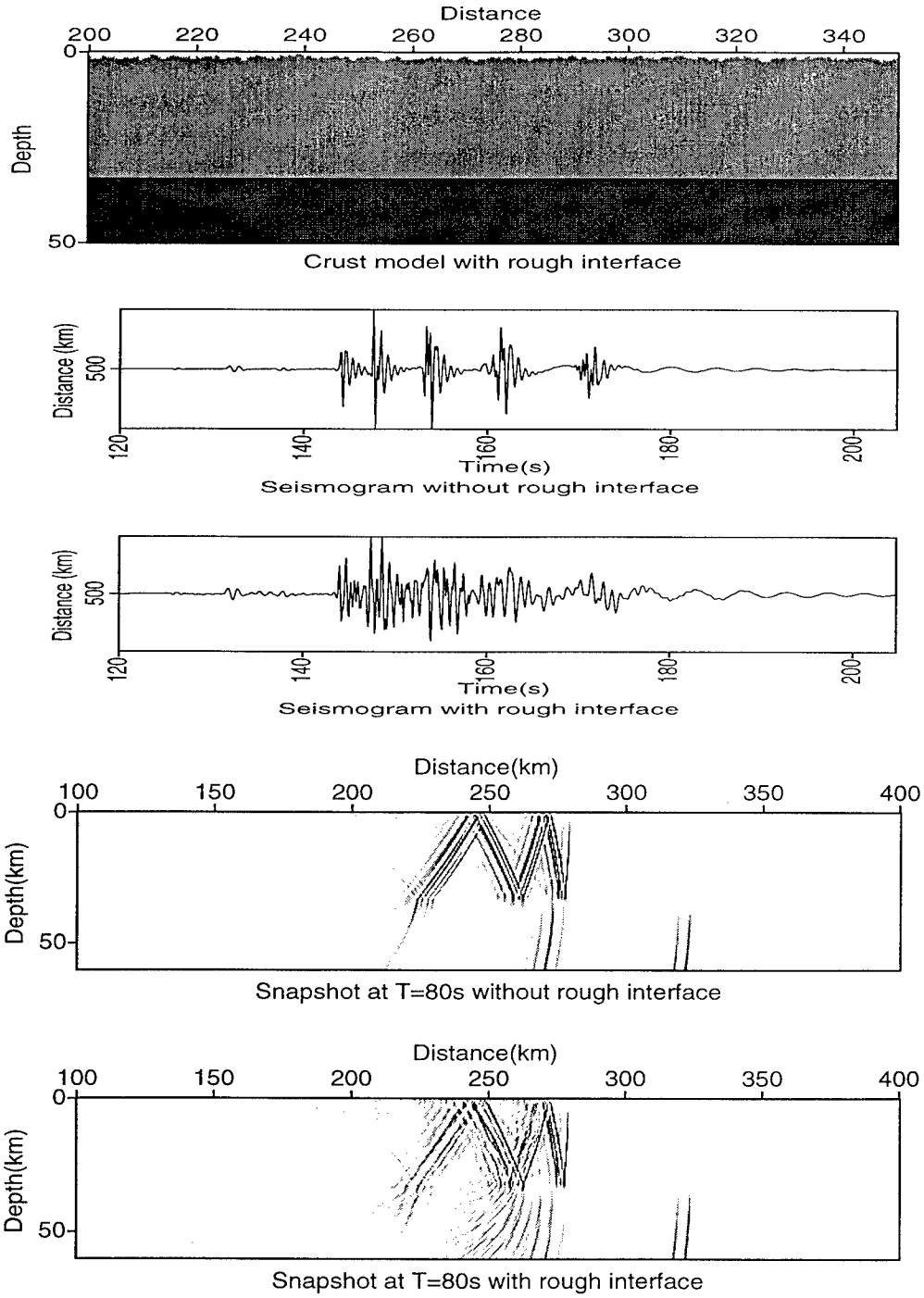

Figure 12: Influence of a rough interface on Lg propagation. The top panel is a crustal model with a sedimentary layer for which the bottom is a rough interface. The second and third panels show the comparison of synthetic seismograms; the bottom two panels show the comparison of snapshots.

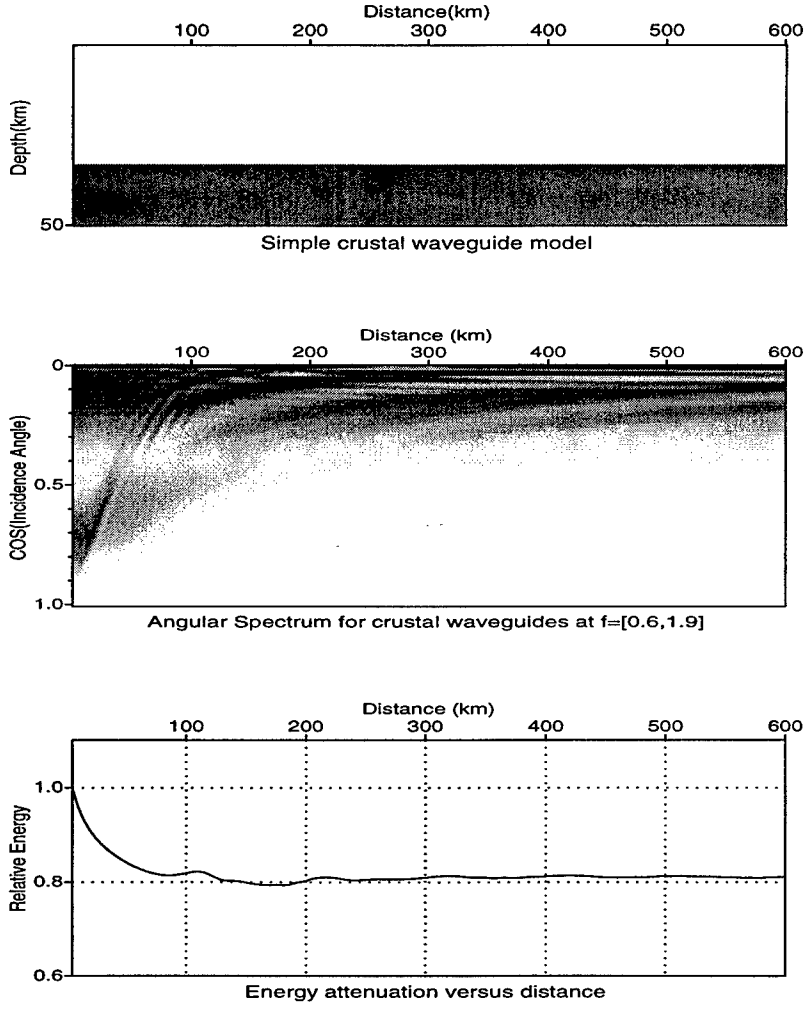

Figure 13: Energy distribution for a uniform crust model. From top to bottom, crustal structure; energy distribution versus vertical slowness and distance; and energy attenuation versus distance.

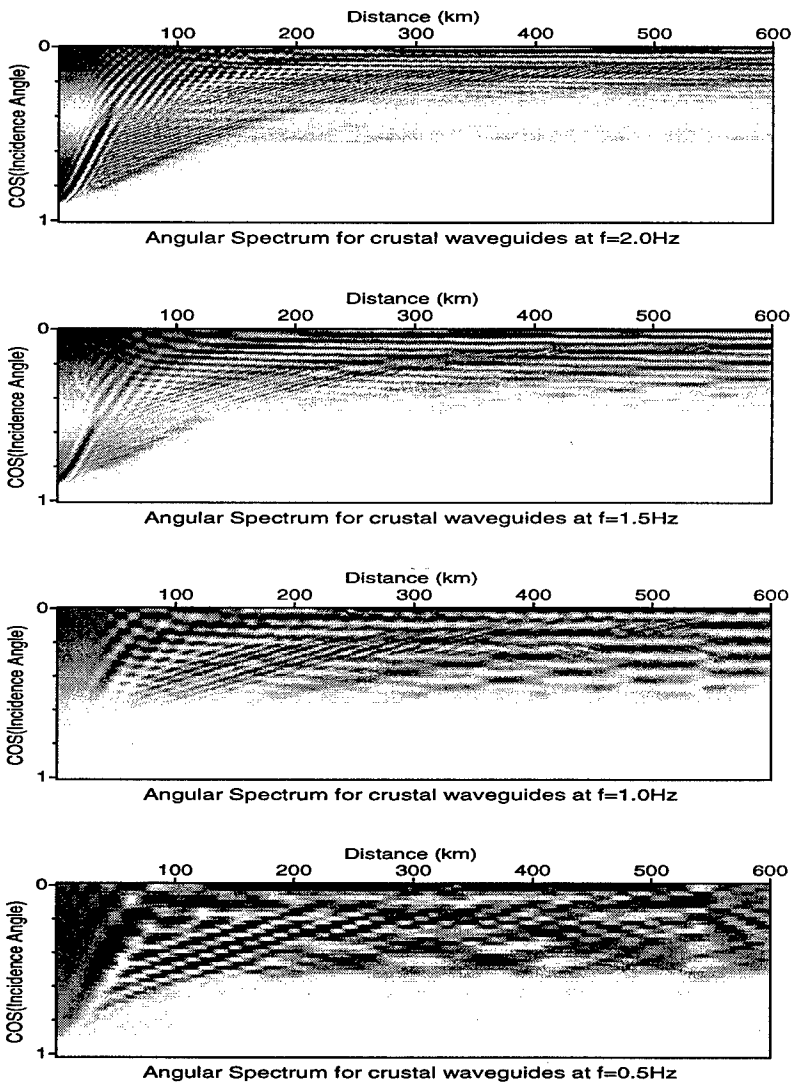

Figure 14: Energy distribution of a uniform crust model versus vertical slowness and distance for different frequencies. From top to bottom, the frequencies are 2.0, 1.5, 1.0 and 0.5 Hz respectively.

5.1 Deterministic waveguide models

Figure 13 shows the result for a simple waveguide. The model is composed of a 30 km thick, horizontal, constant velocity crust over a constant velocity upper mantle. The S-wave velocities and densities are V_1= 3.5 km/s, ρ_1= 2.7 g/cm^3 and V_2= 4.5 km/s, ρ_2= 3.3 g/cm^3 for the crust and upper mantle respectively. Hereafter, we will refer to this model as the reference model. Shown in the upper panel of Figure 13 is the waveguide structure. In the middle is the energy distribution versus the vertical slowness and distance up to 600 km. The vertical coordinate is the normalized vertical slowness K_z/k, corresponding to the cosine of incident angles. Note that zero vertical slowness means horizontal propagation. The frequency range is from 0.6 to 1.9 Hz. At the initial stage, there is considerable energy with large vertical slowness, i.e., with steep angles. After multiple reflections, energy with larger vertical slowness is depleted due to the leakage to the mantle, leaving the energy with small vertical slowness, i.e., the guided waves, propagating in the waveguide. Shown in the lower panel is the wave energy versus the distance. The energy is calculated from synthetic seismograms on the free surface. It can be compared with the observed Lg waves from seismic networks. After the first 100 km, the energy is basically constant. Note that this result is for a two-dimensional range independent waveguide without intrinsic or scattering attenuation. For a real 3D model, the geometrical spreading factor should be different from here. Figure 14 shows the energy distribution versus the vertical slowness and distance for the reference model for individual frequency components. From top to bottom are plots for frequencies 2.0, 1.5, 1.0 and 0.5 Hz, respectively. The energy distribution shows some patterns in the slowness-distance domain. These result from the interference of waves from the source as well as from the free surface and bottom reflections. After a certain distance, the patterns are relatively stable, that is, certain modes have formed in the waveguide and they carry the energy to a long distance. Later we will see the waveguide structures, in both vertical and horizontal directions, can affect the propagating mode, i.e., the patterns of energy distributions.

The second example, shown in Figure 15, is similar to the first one except there is a crust

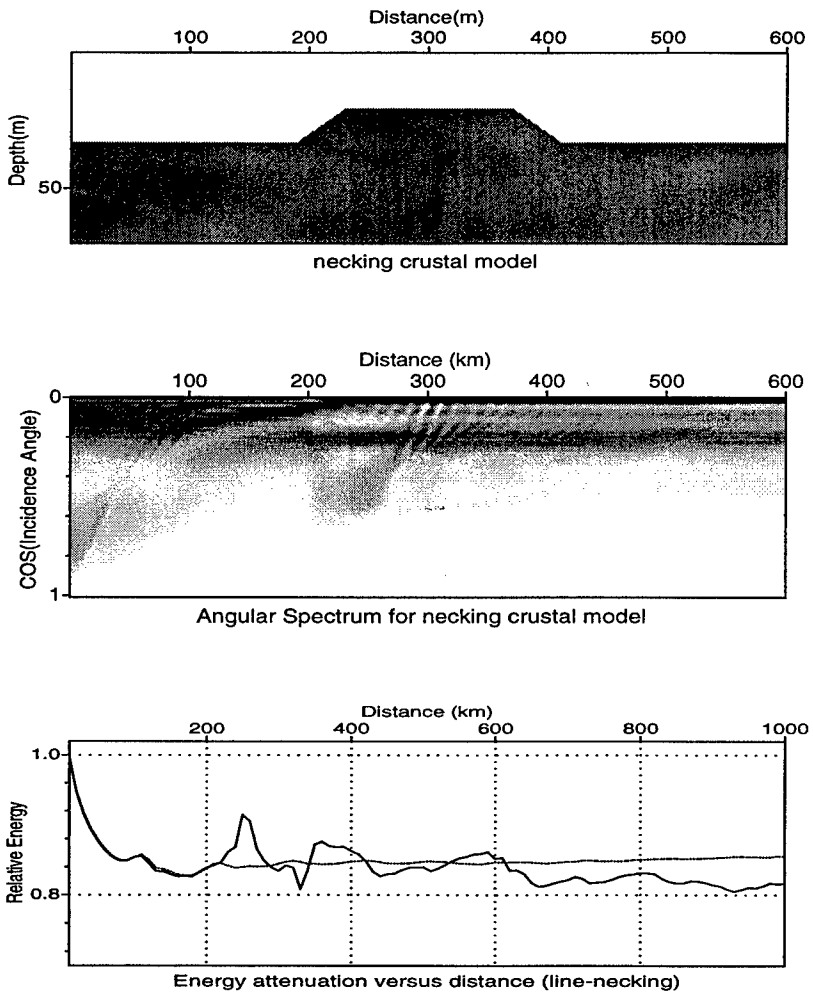

Figure 15: Energy distribution for model with a crustal necking. From top to bottom, crustal structure; energy distribution versus vertical slowness and distance; energy attenuation versus distance.

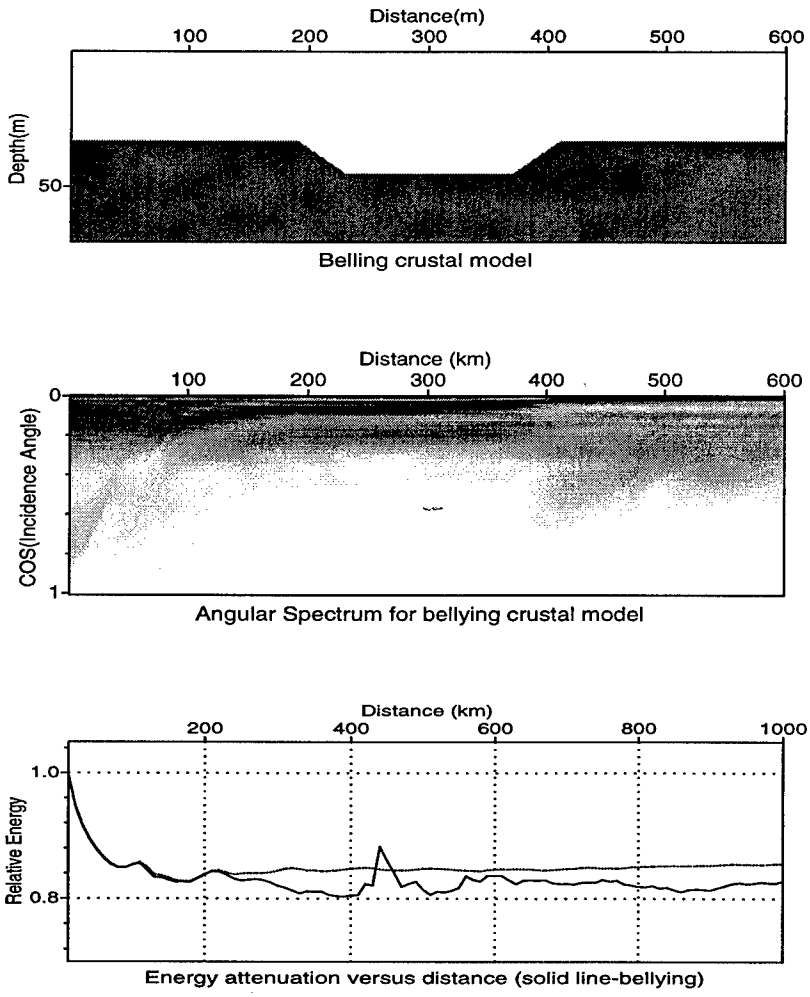

Figure 16: Energy distribution for model with a crustal thickening. From top to bottom, crustal structure; energy distribution versus vertical slowness and distance; and energy attenuation versus distance.

necking in the waveguide where the crust thickness decreased from 30 km to 20 km. The middle panel shows, at the entrance of the necking crust, part of the energy is deflected from its original direction and no longer meets the total reflection condition. This energy finally leaks into the upper mantle and cause attenuation of Lg energy. This can also be seen from the energy attenuation curve in the bottom panel. The model in Figure 16 has a crustal thickening. Again, at the place where the crust thickness decreases (as the wave leaves the exit of the belly), part of the energy is deflected from its original direction and leaked into the upper mantle.

5.2 Waveguide models with random structures

In addition to the large scale, deterministic structures discussed in the above examples, small scale heterogeneities also widely exist in the crust and upper mantle. These small scale structures can be simulated by random velocity fluctuations on a background velocity and by random interface undulations. The following models will be used to test how these small scale structures affect Lg energy transport. Before applying the screen propagator method to a random velocity model, we first check the validity of the screen method by comparing its result with that from a finite-difference method. The upper panel of Figure 17 gives a crust model with 5% RMS velocity perturbation. To shorten the computation time, here we use a 16 km thin crust model. The lower panel shows the comparison of relative attenuation curves between the two methods. The solid line is from a fourth-order finite-difference method and the dotted line is from screen propagator method. The two results give reasonably consistent results. This proves the validity of the screen propagator applied to the energy transfer and partition in random crustal waveguides. For this test model, the FD calculation has $\Delta x = \Delta z = 0.125km$, $\Delta t = 0.015$ sec. resulting in a CPU time of 58 hours on a SUN SPARC-4 work station, while the screen method has $\Delta x = \Delta z = 0.25km$, $\Delta t = 0.1$ sec., and a CPU time 0.5 hour on the same machine. Both calculations have $f_0 = 1$ Hz. For the screen method, the cutoff frequency $f_{max} = 2$ Hz.

Shown in Figure 18 is a normal crustal waveguide similar to the reference model except

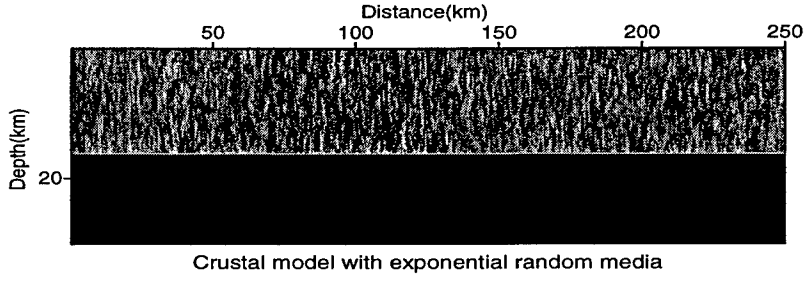

Crustal model with exponential random media

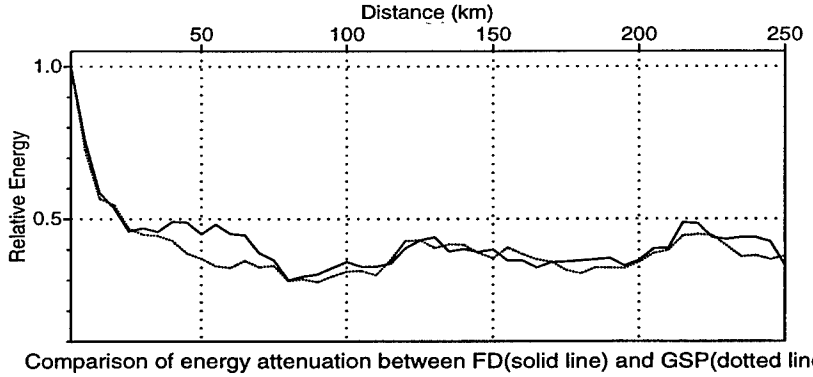

Comparison of energy attenuation between FD(solid line) and GSP(dotted line)

Figure 17: Comparison of energy attenuation curves calculated by screen propagator method and finite-difference method. Shown in the top panel is the velocity structure including random heterogeneities and in the lower panel are the energy attenuation curves.

there is a 5% RMS random velocity perturbation in the crust. The fluctuation has an exponential power spectrum with horizontal and vertical characteristic scales of 5.0 and 3.0 km, respectively. Compared with Figure 13, energy continuously deflects from lower vertical slowness to higher vertical slowness due to the scattering by small scale heterogeneities. This can be seen by comparing the middle panel of Figure 18 with that of Figure 13. In Figure 18 there is more energy seen above the critical wavenumber. The energy with larger vertical slowness tends to leak into the upper mantle and cause additional Lg-wave energy attenuation as can be seen in the lower panel, where the dotted line is for the reference model and solid line is for the random model. Figure 19 is the energy distribution versus slowness and distance for individual frequency components. Comparing with those in Figure 14 for the reference model, we can see that many interference patterns for guided modes are destroyed. This is especially clear for higher frequency components. This phenomenon is also related to the characteristic scale (or equivalently, the spatial power spectrum) of the random heterogeneities. Figure 20 gives the attenuation curves for different characteristic scales. The upper panel is the relative total energy, which is the energy contained in the whole seismogram recorded on the surface versus distance. The solid line is for $ka = 1$, the dotted line is for $ka = 10$, and the dash line is for the reference model. We see that for the reference model, the total energy remains basically constant beyond critical distance, which serves as a checking point for the numerical simulations. The lower panel gives the logarithmic relative RMS Lg wave amplitudes, which are calculated within the Lg window, versus distance. Again, the solid, dash and dotted lines are for $ka = 1$, $ka = 10$ and the reference model. In both measurements $ka = 1$ lines give stronger attenuation than $ka = 10$ lines. We see also that the Lg amplitudes attenuate more rapidly than the total energy. This is due to the effect of scattering, which diffuses the waves out of the Lg window.

The existence of rough surface and interfaces has effects on both excitation and propagation of Lg-waves. First, the rough surface near the source region may affect the source energy partitioning. Second, along the entire propagation path, the trapped energy in the waveguide may be redirected to steeper angles due to scattering, causing it to leak into the upper mantle. This can cause additional Lg-wave attenuation. Similar to the example shown

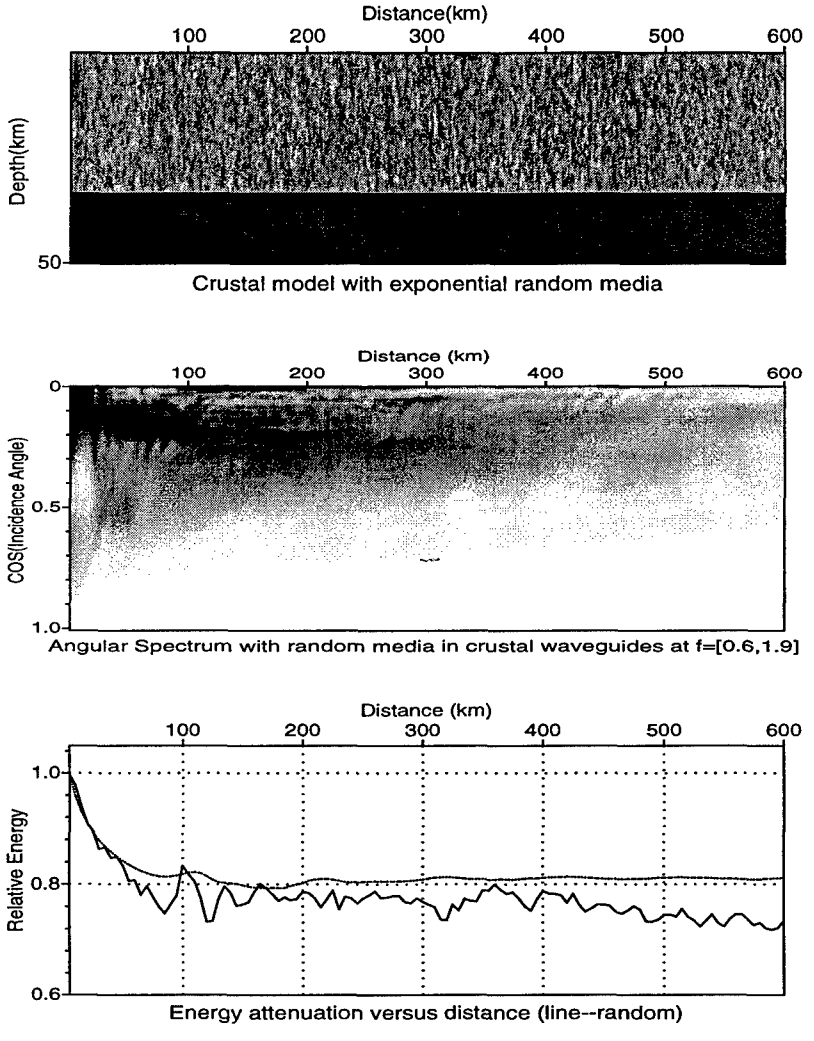

Figure 18: Energy distribution for a crust model with 5% RMS velocity perturbations. From top to bottom, crustal structure; energy distribution versus vertical slowness and distance; energy attenuation versus distance.

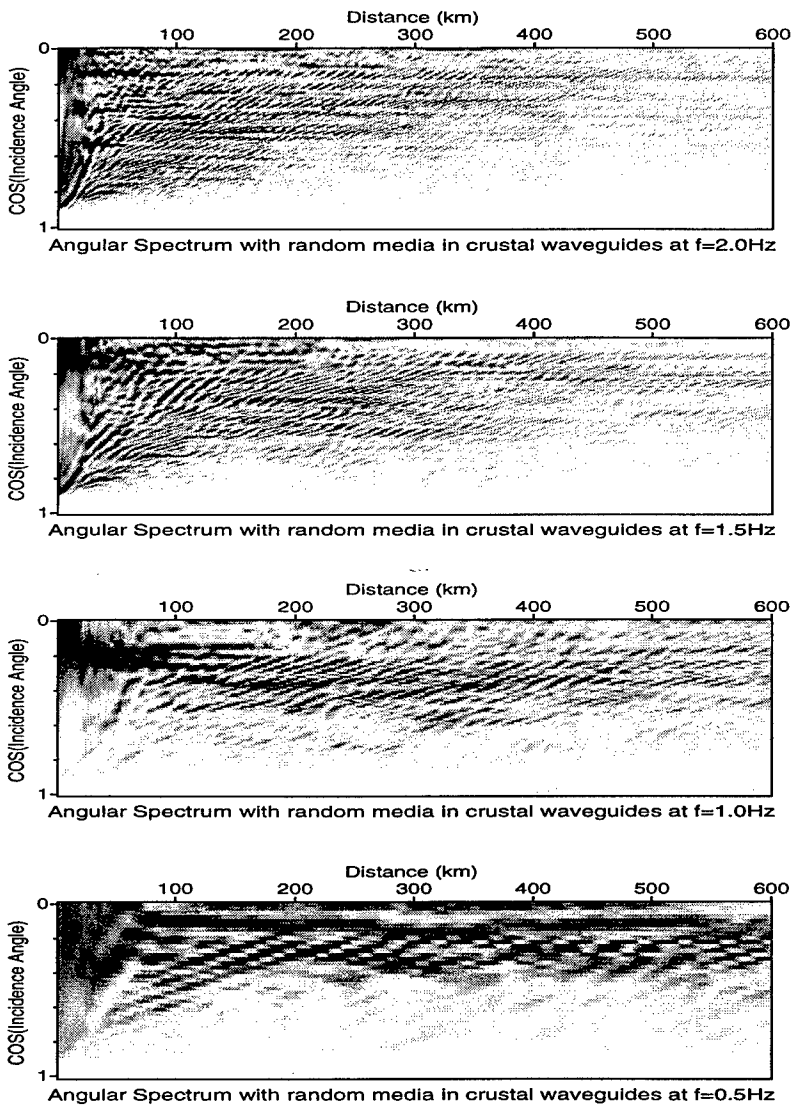

Figure 19: Energy distribution for a crust model with 5% RMS velocity perturbations versus vertical slowness and distance for different frequencies. From top to bottom, the frequencies are 2.0, 1.5, 1.0 and 0.5 Hz respectively.

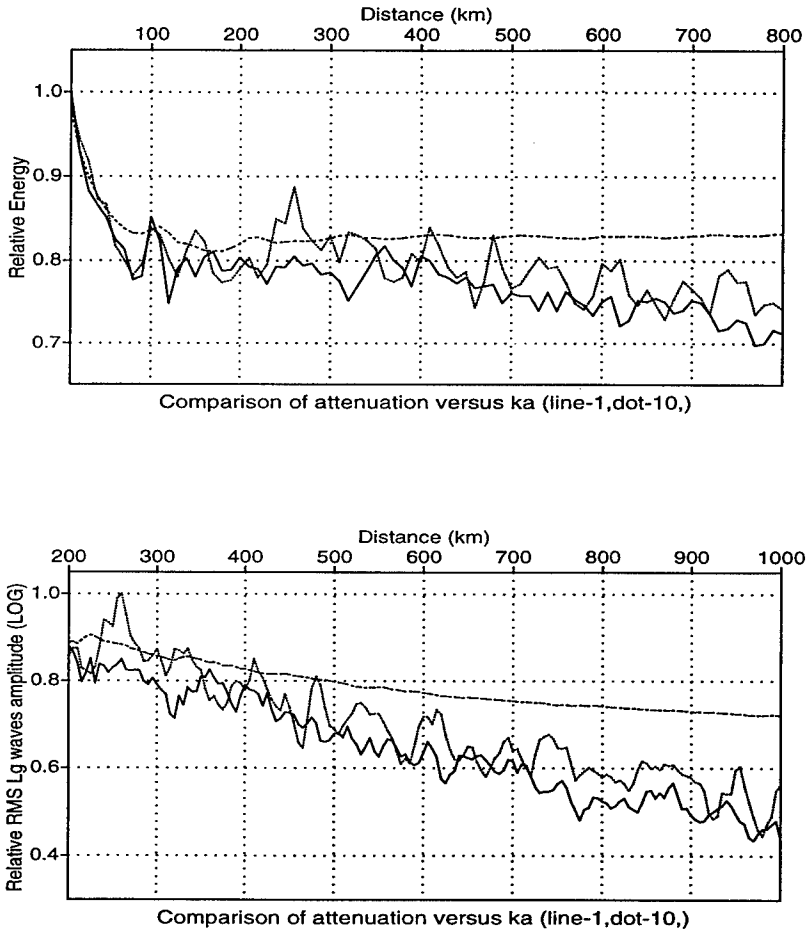

Figure 20: Attenuation curves for different characteristic scales. The upper panel is the relative energy attenuation, and the lower panel is the logarithmic relative RMS Lg wave amplitude attenuation. The solid line is for $ka = 1$, the dotted line is for $ka = 10$, and the dash line is for the reference model.

in the last section, we use a low velocity layer with a rough lower interface to simulate the effect of a rough surface. In Figure 21, the upper panel is the velocity structure including a surface sedimentary layer with a random interface. The sedimentarylayer has an average thickness of 1 km and a RMS depth perturbation of 0.2 km with correlation length of 1 km. The middle panel is the energy distribution versus distance and vertical slowness. Compared with Figure 13 for the reference model, it clearly shows, with the existence of a rough interface, considerable energy moves from lower vertical slowness to higher vertical slowness. In other words, the energy propagation directions are deflected from near horizontal to steeper directions, which makes more energy leak into the upper mantle and causes extra Lg wave attenuation. The lower panel gives the energy attenuation curves versus distance, in which the solid line is for the model with rough interface and the dotted line is for the reference model. It shows clearly the effect of rough interface on Lg attenuation.

6 Conclusion

The advantages of the half-space GSP method can be summarized as follows.

- **Fast speed:** For medium size 2D Lg problems, it is 2-3 orders of magnitude faster than the FD methods. For large distance, high frequency 3D problems, the time saving factor could be much greater.
- **Memory saving**: The *GSP* needs only to store 2D data arrays for each step instead of 3D volume data, leading to huge memory savings.
- **Stability**: The transversal Laplacian is calculated by the Fourier method, therefore no numerical dispersion occurs for high frequency waves.
- **Intrinsic attenuation**: Being a frequency domain method, it is easy to incorporate various Q models into the simulation. Therefore, the method can study the effects of scattering and anelasticity on Lg wave blockage and attenuation.

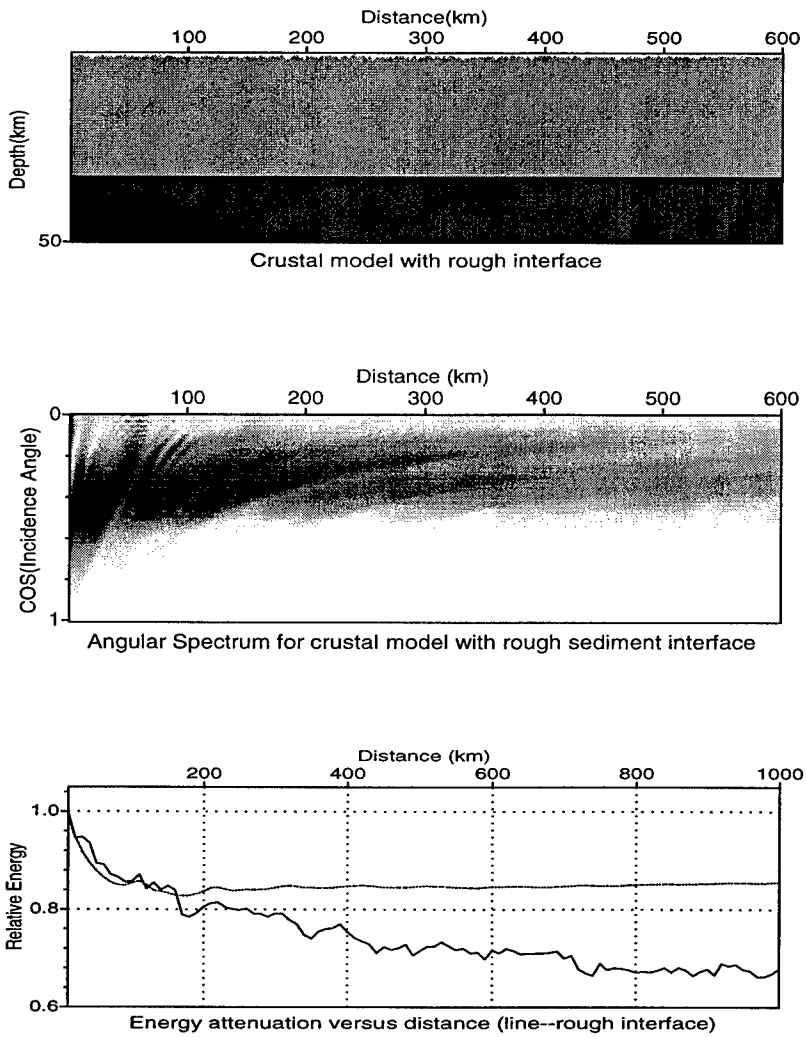

Figure 21: Energy distribution for a crustal waveguide model with rough interface. From top to bottom, crustal structure; energy distribution versus vertical slowness and distance; and energy attenuation versus distance.

- **Random heterogeneities and rough interfaces**: Random heterogeneities and rough interfaces can also be easily incorporated into the model. The effects of small scale heterogeneities and rough interfaces, and their statistical characteristics can be studied by numerical simulations using this method.

The use of half-space phase-screen propagator has made seismogram synthesis at regional distances very efficient. Rapid changes of crustal structure and small scale heterogeneities and rough interfaces in the crust can be easily handled. The results in this paper demonstrates the advantages and feasibility of the approach. P-SV and full 3D problems will be treated in future work.

7 References

Aki, K., and P.G. Richards, *Quantitative Seismology: Theory and Methods, Vol. 1 and 2*, W.H. Freeman, New York, 1980.

Baumgardt, D.R., Investigation of teleseismic Lg blockage and scattering using regional arrays, *Bull. Seismol. Soc. Am., 80*, 2261-2281, 1990.

Bouchon, M., et al., Theoretical modeling of Lg wave attenuation, in *The VELA Program; A Twenty-five Year Review of Basic Research,* 1985.

Campillo, M., Propagation and attenuation characteristics of the crustal phase Lg, *Pure and Appl. Geophys., 132*, 1-19, 1990.

Campillo, M. and A. Paul, Influence of lower crustal structure on the early coda of regional seismograms, *J. Geophys. Res., 97*, 3405-3416, 1992.

Campillo, M., B. Feignier, M. Bouchon and N. Bethoux, Attenuation of crustal waves across the Alpine range, *J. Geophys. Res., 98*, 1987-1996, 1993.

De Wolf, D.A., Electromagnetic reflection from an extended turbulent medium: cumulative forward-scatter single-backscatter approximation, *IEEE trans. Ant. and Propag., AP-19*, 254-262, 1971.

De Wolf, D.A., Renormalization of EM fields in application to large-angle scattering from randomly continuous media and sparse particle distributions, *IEEE trans. Ant. and Propag., AP-33*, 608-615, 1985.

Frankel, A., A review of numerical experiments on seismic wave scattering, in *Scattering and Attenuation of Seismic Waves, II,* edited by R.S. Wu and K. Aki, pp. 639-686, Birkhauser, Berlin, 1989.

Frankel, A. and R.W. Clayton, Finite difference simulations of seismic scattering: Implications for propagation of short-period seismic waves in the crust and models of crustal heterogeneity, *J. Geophys. Res., 91*, 6465-6489, 1986.

Gibson, R.L. M. Campillo, 1994, Numerical simulation of high- and low-frequency Lg-wave propagation, *Geophys. J. Int., 118*, 47-56, 1994.

Goldstein, P., C. Schultz, S. Larsen and L. Minner, Modeling of regional wave propaga-

tion phenomena in the middle east and north Africa and new analysis capabilities in SAC2000, *Proceedings of the 18th Annual Seismic Research Smposium on Monitoring a Comprehensive Test Ban Treaty*, 165-171, September 4-6, 1996.

Holliger, K. and A.R. Levander, A stochastic view of lower crustal fabric based on evidence from the Ivrea zone, *Geophys. Res. Lett., 19*, 1153-1156, 1992.

Huang, L.J. and R.S. Wu, 3D prestack depth migration with acoustic pseudo-screen propagators, *Mathematical methods in geophysical imaging IV, SPIE, 2822*, 40-51, 1996.

Jih, R.S., Waveguide Effects of large-scale structural variation, anelastic attenuation, and random heterogeneity on SV Lg propagation: a finite-difference modeling study, *Proceedings of the 18th Annual Seismic Research Smposium on Monitoring a Comprehensive Test Ban Treaty*, 182-194, September 4-6, 1996.

Kennet, B.L.N., Lg-wave propagation in heterogeneous media, *Bull. Seismol. Soc. Am., 79*, 860-872, 1989.

Kennet, B.L.N., Guided wave attenuation in laterally varying media, *Geophys. J. Int., 100*, 415-422, 1990.

Kosloff, D., D. Kessler, A. Quieroz, and E. Tessmer, Solution of the equations of Dynamic elasticity by a Chebychev spectral method, *Geophysics, 55*, 734-748, 1990.

Levander, A.. and K. Holliger, Small-scale heterogeneity and large-scale velocity structure of the continental crust, *J. Geophys. Res., 97*, 7897-8804, 1992.

Liu, Y.B. and R.S. Wu, A comparison between phase-screen, finite difference and eigenfunction expansion calculations for scalar waves in inhomogeneous media, *Bull. Seis. Soc. Am., 84*, 1154-1168, 1994.

Maupin V., Numerical modeling of Lg wave propagation across the North Sea central graben, *Geophys. J. Int., 99*, 273-283, 1989.

Morse, P.M., and H. Feshbach, *Methods of Theoretical Physics*, chapter 7, McGraw-Hill Book Comp., New York, 1953.

Orrey, J., C. Archambeau and G. Frazier, Complete seismic wave field synthesis with a pseudospectral method: the generalized Fourier method, *Geophys. J. Int.*, 1996.

Schatzman, J.C., A pseudo-spectral scheme for viscoelastic seismic modeling, *Proceedings of*

the 18th Annual Seismic Research Smposium on Monitoring a Comprehensive Test Ban Treaty, 261-270, September 4-6, 1996.

Wu, R.S., Wide-angle elastic wave one-way propagation in heterogeneous media and an elastic wave complex-screen method, *J. Geophys. Res., 99*, 751-766, 1994.

Wu, R.S., Synthetic seismograms in heterogeneous media by one-return approximation, *Pure and Applied Geophysics, 148*, 155-173, 1996.

Wu, R.S., and L.J. Huang, Reflected wave modeling in heterogeneous acoustic media using the de Wolf approximation, *Mathematical Methods in Geophysical Imaging III, SPIE Proceedings Series, 2571*, 176-186, 1995.

Wu, R.S. and X.B., Xie, Multi-screen backpropagator for fast 3D elastic prestack migration, *Mathematical Methods in Geophysical Imaging II, SPIE Proceedings Series, 2301*, 181-193, 1994.

Wu, R.S., Z. Xu, and X.P. Li, Heterogeneity spectrum and scale-anisotropy in the upper crust revealed by the German continental deep-drilling (KTB) holes, *Geophys. Res. Lett., 21*, 911-914, 1994.

Wu, R.S., S. Jin, X.B. Xie, Seismic wave propagation and scattering in heterogeneous crustal waveguides using screen propagators: I SH-waves, *Proceeding of 18th Annual Seismic Research Symposium on Monitoring a Comprehensive Test Ban Treaty*, 291-300, 1996.

Wu, R.S., S. Jin, X.B. Xie, and T. Lay, Verification and applications of GSP (Generalized screen propagators) method for regional wave propagation, *Proceeding of 19th Annual Seismic Research Symposium on Monitoring a Comprehensive Test Ban Treaty*, 552-561, 1997.

Wu, R.S., S. Jin and X.B. Xie, Seismic wave propagation and scattering in heterogeneous crustal waveguides using screen propagators: I SH-waves, submitted to *J. Geophys. Res.*, 1997.

Xie, X.B. and T. Lay, The excitation of explosion Lg, a finite-difference investigation, *Bull. Seismol. Soc. Am., 84*, 324-342, 1994.

Xie, X.B. and R.S. Wu, A complex-screen method for modeling elastic wave reflections, *Expanded Abstracts, SEG 65th Annual Meeting*, 1269-1272, 1995.

Xie, X.B. and R.S. Wu, 3D elastic wave modeling using the complex screen method, *Expanded Abstracts, SEG 66th Annual Meeting*, 1247-1250, 1996.